To determine if this protease activity degrades the extracellular or intracellular domain of βDG, we prepared the fusion proteins corresponding to the extracellular domain (βDGext) and intracellular domain (βDGint) of βDG. We incubated βDGext and βDGint with the total RT4 cell homogenate as well as the RT4 cell culture medium concentrated to the same volume as the total cell homogenate. When βDGext was incubated with the cell homogenate or culture medium, it was degraded progressively (Fig. 2a). However, the degradation of βDGext was more prominent with the cell culture medium than cell homogenate (Fig. 2a). These results indicate that the protease activity that degrades βDGext is more abundant in the cell culture medium than cells themselves. On the other hand, βDGint was not degraded at all, when it was incubated with either the RT4 cell homogenate or the concentrated culture medium (Fig. 2b). To further confirm the specificity of degradation of the extracellular domain of βDG, we prepared various fusion proteins, including αDG N-ter, αDG C-ter, Dys, and GST. None of them were degraded, when they were incubated with either the RT4 cell homogenate or the concentrated culture medium (Fig. 2b). Altogether, these results indicate that the RT4 cell culture medium is enriched with the protease activity that degrades the extracellular domain of βDG specifically.

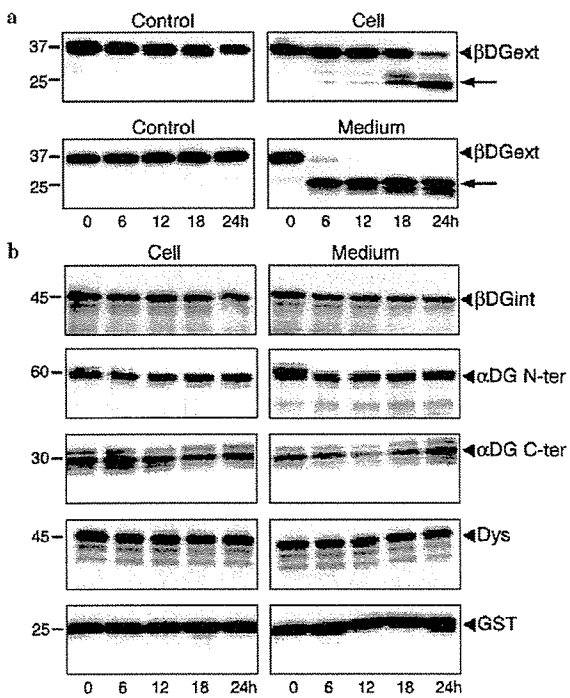

Fig. 2. Specific degradation of βDGext by RT4 cell homogenate and culture medium. (a) βDGext was incubated with the total RT4 cell homogenate as well as the RT4 cell culture medium concentrated to the same volume as the total cell homogenate for various time periods, and analyzed by immunoblotting using anti-GST-HRP conjugate. For controls, βDGext was incubated with the cell homogenization buffer and the concentrated control medium, respectively. The bands indicated by arrows are presumed degradation products of βDGext, because they were detected by anti-GST-HRP conjugate. (b) βDGint, αDG N-ter, αDG C-ter, Dys, and GST were incubated with the RT4 cell homogenate and culture medium for various time periods, and analyzed by immunoblotting using anti-GST-HRP conjugate. Molecular mass standards (Da × 10^3) are shown on the left.

Effects of MMP inhibitors on the degradation of βDGext by the concentrated RT4 cell culture medium

To see if MMPs are involved in the degradation of βDGext, we incubated βDGext with the concentrated RT4 cell culture medium in the presence or absence of inhibitors of MMP-2/MMP-9, MMP-1/MMP-8, MMP-3, and MMP-13 [15–18]. The degradation of βDGext was significantly reduced only by the inhibitor of MMP-2/MMP-9, but not by the inhibitor of MMP-1/MMP-8, MMP-3 or MMP-13 (Fig. 3).

Expression of MMP-2 and MMP-9 in RT4 cells and cell culture medium

To see if MMP-2 and MMP-9 are expressed in RT4 cells and cell culture medium, we performed zymographic analysis of MMP-2 and MMP-9. The 66 kDa band of activated MMP-2 and the 83 kDa band of activated MMP-9 were

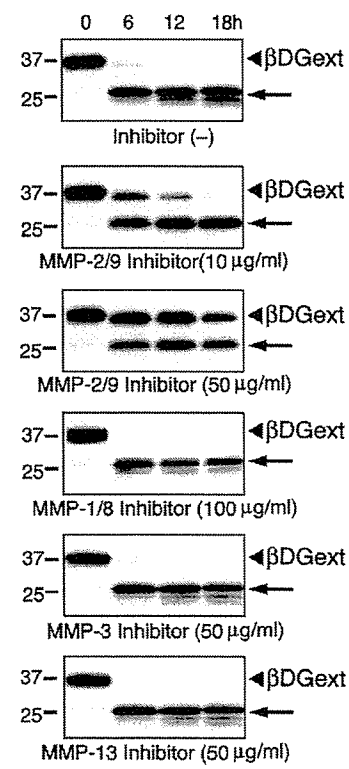

Fig. 3. Effects of MMP inhibitors on the degradation of βDGext. βDGext was incubated with the concentrated RT4 cell culture medium in the absence or presence of inhibitors of various MMPs and analyzed by immunoblotting using anti-GST-HRP conjugate. The bands indicated by arrows are presumed degradation products of βDGext, because they were detected by anti-GST-HRP conjugate. Molecular mass standards (Da × 10^3) are shown on the left.

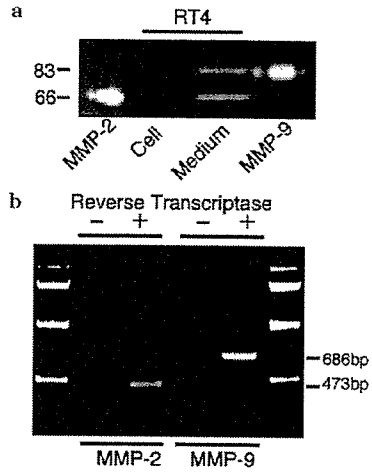

Fig. 4. Expression of MMP-2 and MMP-9 in RT4 cells and RT4 cell culture medium. (a) Zymography of RT4 cells and RT4 cell culture medium. RT4 cell homogenate and culture medium, as well as active human MMP-2 and recombinant human MMP-9, were applied for zymography. Molecular mass standards (Da × 10^3) are shown on the left. (b) RT-PCR analysis of the total RNA from RT4 cells. mRNAs for MMP-2 and MMP-9 were amplified in the presence or absence of reverse transcriptase.

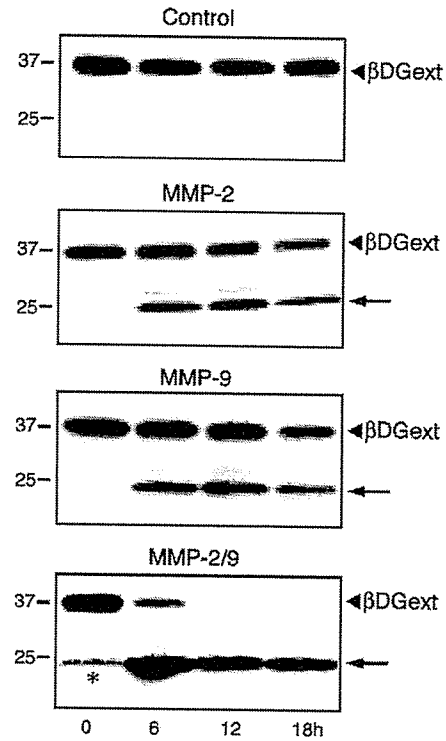

Fig. 5. Degradation of βDGext by active MMP-2 and MMP-9 enzymes. Forty nanograms/microliter of βDGext was incubated with 2 ng/μl of active human MMP-2 and recombinant human MMP-9 for various time periods. Samples were analyzed by immunoblotting using anti-GST-HRP conjugate. The bands indicated by arrows are presumed degradation products of βDGext, because they were detected by anti-GST-HRP conjugate. The band indicated by the asterisk in the lane of 0 h is an overflow from the lane of 6 h. Molecular mass standards (Da × 10^3) are shown on the left.

detected in the RT4 cell culture medium, while they were not detected in the total RT4 cell homogenate (Fig. 4a). We performed RT-PCR analysis of the total RNA from RT4 cells. A single PCR fragment of the expected size was detected for both MMP-2 and MMP-9 (Fig. 4b). We excised and subcloned the PCR products and confirmed that the products had the sequence of rat MMP-2 and MMP-9 (data not shown). These results indicate the de novo synthesis of MMP-2 and MMP-9 in RT4 cells and their secretion into the culture medium.

Degradation of βDGext by MMP-2 and MMP-9

To see if MMP-2 and MMP-9 are involved in the processing of βDG, we incubated βDGext with the active enzymes of MMP-2 and MMP-9. βDGext was degraded progressively by the incubation with either MMP-2 or MMP-9 (Fig. 5). Moreover, the degradation of βDGext was augmented significantly when it was incubated with both MMP-2 and MMP-9 (Fig. 5).

Discussion

In this study, we found that the culture medium of RT4 cells was enriched with the protease activity that degrades the fusion protein construct of the extracellular domain of βDG specifically. This activity was suppressed by the inhibitor of MMP-2 and MMP-9, but not by the inhibitors of MMP-1, MMP-3, MMP-8, and MMP-13. Zymography and RT-PCR analysis showed that RT4 cells secreted MMP-2 and MMP-9 into the culture medium. Finally, active MMP-2 and MMP-9 enzymes degraded the fusion protein construct of the extracellular domain of βDG. These results indicate (1) that RT4 cells secrete the protease activity that degrades the extracellular domain of βDG specifically and (2) that MMP-2 and MMP-9 may be involved in this process.

Disruption of the link between the ECM and cell membrane via the DG complex is presumed to have a deleterious effect on the stability of cell membrane and viability of cells [6]. MMPs are the candidate molecules that degrade the components of the DG complex and disrupt this link [6–13]. In this context, it is noteworthy that MMPs have been implicated in the molecular pathogenesis of muscular dystrophies. von Moers et al. reported that gelatinolytic activity of MMP-2 was increased in the skeletal muscle of DMD [19]. Kherif et al. reported that both pro and active forms of MMP-2 and MMP-9 were expressed in the skeletal muscle of *mdx* mice [20]. Lattanzi et al. reported the aberrantly processed laminin α2 chain and increased activity of MMP-2/MMP-14 in the cultured skeletal muscle cells of congenital muscular dystrophy [21]. Interestingly, it has recently been reported that the processing of DG by MMP-2 and MMP-9 may be involved in the leukocyte extravasation in experimental autoimmune encephalomyelitis [22].

The present study, which demonstrates the secretion of the protease activity that degrades the extracellular domain of βDG by cultured cells and points to the roles of MMP-2 and MMP-9 in this process, would further help to broaden our understanding of the complex mechanisms involved in the processing of βDG.

Acknowledgments

We thank Miki Yamanaka and Yuka Sasayama for their expert technical assistance. This work was supported by [1] Research Grants 16B-1 and 17A-10 for Nervous and Mental Disorders (Ministry of Health, Labor and Welfare), [2] Research on Psychiatric and Neurological Diseases and Mental Health (Ministry of Health, Labor and Welfare), and [3] Research Grants 16390256, 40286993, and "Open Research Center" Project for Private Universities: matching fund subsidy from MEXT (Ministry of Education, Culture, Sports, Science, and Technology), 2004–2008.

References

[1] O. Ibraghimov-Beskrovnaya, J.M. Ervasti, C.J. Leveille, C.A. Slaughter, S.W. Sernett, K.P. Campbell, Primary structure of dystrophin-associated glycoproteins linking dystrophin to the extracellular matrix, Nature 355 (1992) 696–702.

[2] M.D. Henry, K.P. Campbell, Dystroglycan: an extracellular matrix receptor linked to the cytoskeleton, Curr. Opin. Cell Biol. 8 (1996) 625–631.

[3] J.M. Ervasti, K.P. Campbell, Membrane organization of the dystrophin-glycoprotein complex, Cell 66 (1991) 1121–1131.

[4] A. Suzuki, M. Yoshida, K. Hayashi, Y. Mizuno, Y. Hagiwara, E. Ozawa, Molecular organization at the glycoprotein-complex-binding-site of dystrophin. Three dystrophin-associated proteins bind directly to the carboxy-terminal portion of dystrophin, Eur. J. Biochem. 220 (1994) 283–292.

[5] E. Di Stasio, F. Sciandra, B. Maras, F. Di Tommaso, T.C. Petrucci, B. Giardina, A. Brancaccio, Structural and functional analysis of the N-terminal extracellular region of β-dystroglycan, Biochem. Biophys. Res. Commun. 206 (1999) 274–278.

[6] H. Yamada, F. Saito, H. Fukuta-Ohi, D. Zhong, A. Hase, K. Arai, A. Okuyama, R. Maekawa, T. Shimizu, K. Matsumura, Processing of β-dystroglycan by matrix metalloproteinase disrupts the link between the extracellular matrix and cell membrane via the dystroglycan complex, Hum. Mol. Genet. 15 (2001) 1563–1569.

[7] K. Matsumura, K. Arai, D. Zhong, F. Saito, H. Fukuta-Ohi, R. Maekawa, H. Yamada, T. Shimizu, Disruption of dystroglycan axis by β-dystroglycan processing in cardiomyopathic hamster muscle, Neuromuscul. Disord. 13 (2003) 796–803.

[8] K. Matsumura, D. Zhong, F. Saito, K. Arai, K. Adachi, H. Kawai, I. Higuchi, I. Nishino, T. Shimizu, Proteolysis of β-dystroglycan in muscular diseases, Neuromuscul. Disord. 15 (2005) 336–341.

[9] C. Herzog, C. Has, C.W. Franzke, F.G. Echtermeyer, U. Schlotzer-Schrehardt, S. Kroger, E. Gustafsson, R. Fassler, L. Bruckner-Tuderman, Dystroglycan in skin and cutaneous cells: β-subunit is shed from the cell surface, J. Invest. Dermatol. 122 (2004) 1372–1380.

[10] C. Losasso, F. Di Tommaso, A. Sgambato, R. Ardito, A. Cittadini, B. Giardina, T.C. Petrucci, A. Brancaccio, Anomalous dystroglycan in carcinoma cell lines, FEBS Lett. 484 (2000) 194–198.

[11] A. Sgambato, M. Migaldi, M. Montanari, A. Camerini, A. Brancaccio, G. Rossi, R. Cangiano, C. Losasso, G. Capelli, G.P. Trentini, A. Cittadini, Dystroglycan expression is frequently reduced in human breast and colon cancers and is associated with tumor progression, Am. J. Pathol. 162 (2003) 849–860.

[12] J. Jing, C.F. Lien, S. Sharma, J. Rice, P.A. Brennan, D.C. Gorecki, Aberrant expression, processing and degradation of dystroglycan in squamous cell carcinomas, Eur. J. Cancer 40 (2004) 2143–2151.

[13] L. Leone, M.E. De Stefano, A. Del Signore, T.C. Petrucci, P. Paggi, Axotomy of sympathetic neurons activates the metalloproteinase-2 enzymatic pathway, J. Neuropathol. Exp. Neurol. 64 (2005) 1007–1017.

[14] F. Saito, T. Masaki, K. Kamakura, L.V.B. Anderson, S. Fujita, H. Fukuta-Ohi, Y. Sunada, T. Shimizu, K. Matsumura, Characterization of the transmembrane molecular architecture of the dystroglycan complex in schwann cells, J. Biol. Chem. 274 (1999) 8240–8246.

[15] Y. Tamura, F. Watanabe, T. Nakatani, K. Yasui, M. Fuji, T. Komurasaki, H. Tsuzuki, R. Maekawa, T. Yoshioka, K. Kawada, K. Sugita, M. Ohtani, Highly selective and orally active inhibitors of type IV collagenase (MMP-9 and MMP-2): *N*-sulfonylamino acid derivatives, J. Med. Chem. 41 (1998) 640–649.

[16] R. Hanemaaijer, T. Sorsa, Y.T. Konttinen, Y. Ding, M. Sutinen, H. Visser, V.W. van Hinsbergh, T. Helaakoski, T. Kainulainen, H. Ronka, H. Tschesche, T. Salo, Matrix metalloproteinase-8 is expressed in rheumatoid synovial fibroblasts and endothelial cells. Regulation by tumor necrosis factor-α and doxycycline, J. Biol. Chem. 272 (1997) 31504–31509.

[17] N. Fotouhi, A. Lugo, M. Visnick, L. Lusch, R. Walsky, J.W. Coffey, A.C. Hanglow, Potent peptide inhibitors of stromelysin based on the prodomain region of matrix metalloproteinases, J. Biol. Chem. 269 (1994) 30227–30231.

[18] J.M. Chen, F.C. Nelson, J.I. Levin, D. Mobilio, F.J. Moy, R. Nilakantan, A. Zask, R. Powers, Structure-based design of a novel, potent, and selective inhibitor for MMP-13 utilizing NMR spectroscopy and computer-aided molecular design, J. Am. Chem. Soc. 122 (2000) 9648–9654.

[19] A. von Moers, A. Zwirner, A. Reinhold, O. Bruckmann, F. van Landeghem, G. Stoltenburg-Didinger, D. Schuppan, H. Herbst, M. Schuelke, Increased mRNA expression of tissue inhibitors of metalloproteinase-1 and -2 in Duchenne muscular dystrophy, Acta Neuropathol. 109 (2005) 193–285.

[20] S. Kherif, C. Lafuma, M. Dehaupas, S. Lachkar, J.G. Fournier, M. Verdiere-Sahuque, M. Fardeau, H.S. Alameddine, Expression of matrix metalloproteinases 2 and 9 in regenerating skeletal muscle: a study in experimentally injured and mdx muscles, Dev. Biol. 205 (1999) 158–170.

[21] G. Lattanzi, F. Muntoni, P. Sabatelli, S. Squarzoni, N.M. Maraldi, V. Cenni, M. Villanova, M. Columbaro, L. Merlini, S. Marmiroli, Unusual laminin α2 processing in myoblasts from a patient with a novel variant of congenital muscular dystrophy, Biochem. Biophys. Res. Comm. 277 (2000) 639–642.

[22] S. Agrawal, P. Anderson, M. Durbeej, N. van Rooijen, F. Ivars, G. Opdenakker, L.M. Sorokin, Dystroglycan is selectively cleaved at the parenchymal basement membrane at sites of leukocyte extravasation in experimental autoimmune encephalomyelitis, J. Exp. Med. (2006), Epub ahead of print.

Journal of Neurochemistry, 2007

doi:10.1111/j.1471-4159.2007.04462.x

Defective peripheral nerve myelination and neuromuscular junction formation in fukutin-deficient chimeric mice

Fumiaki Saito,* Toshihiro Masaki,† Yuko Saito,* Ayami Nakamura,* Satoshi Takeda,‡ Teruo Shimizu,* Tatsushi Toda§ and Kiichiro Matsumura*

**Department of Neurology and Neuroscience, Teikyo University, Tokyo, Japan*

†Department of Neurology, National Institute on Alcoholism, Kurihama National Hospital, Kanagawa, Japan

‡Otsuka GEN Research Institute, Otsuka Pharmaceutical Co. Ltd, Tokushima, Japan

§Division of Clinical Genetics, Department of Medical Genetics, Osaka University Graduate School of Medicine, Osaka, Japan

Abstract

Dystroglycan is a central component of the dystrophin–glycoprotein complex that links the extracellular matrix with cytoskeleton. Recently, mutations of the genes encoding putative glycosyltransferases were identified in several forms of congenital muscular dystrophies accompanied by brain anomalies and eye abnormalities, and aberrant glycosylation of α-dystroglycan has been implicated in their pathogeneses. These diseases are now collectively called α-dystroglycanopathy. In this study, we demonstrate that peripheral nerve myelination is defective in the fukutin-deficient chimeric mice, a mouse model of Fukuyama-type congenital muscular dystrophy, which is the most common α-dystroglycanopathy in Japan. In the peripheral nerve of these mice, the density of myelinated nerve fibers was significantly decreased and clusters of abnormally large non-myelinated axons were ensheathed by a single Schwann cell, indicating a defect of the radial sorting mechanism. The sugar chain moiety and laminin-binding activity of α-dystroglycan were severely reduced, while the expression of β1-integrin was not altered in the peripheral nerve of the chimeric mice. We also show that the clustering of acetylcholine receptor is defective and neuromuscular junctions are fragmented in appearance in these mice. Expression of agrin and laminin as well as the binding activity of α-dystroglycan to these ligands was severely reduced at the neuromuscular junction. These results demonstrate that fukutin plays crucial roles in the myelination of peripheral nerve and formation of neuromuscular junction. They also suggest that defective glycosylation of α-dystroglycan may play a role in the impairment of these processes in the deficiency of fukutin.

Keywords: dystroglycan, fukutin, glycosylation, myelination, neuromuscular junction.

J. Neurochem. (2007) 10.1111/j.1471-4159.2007.04462.x

Dystroglycan (DG) is encoded by a single gene and cleaved into two proteins, α- and β-DG, by post-translational processing (Ibraghimov-Beskrovnaya *et al.* 1992). In skeletal muscle, DG is a key component of the dystrophin–glycoprotein complex (DGC). α-DG is a highly glycosylated extracellular peripheral membrane protein that binds to several extracellular matrix (ECM) proteins, such as laminin, agrin, and perlecan (Ervasti and Campbell 1993; Bowe *et al.* 1994; Peng *et al.* 1998). The mucin-like domain of α-DG binds to laminin G like domains of these ligands (Kanagawa *et al.* 2004) and certain sugar chain structures of α-DG, including Siaα2–3Galβ1–4GlcNAcβ1–2Man–Ser/Thr, are involved in this binding (Chiba *et al.* 1997). On the other hand, the transmembrane protein β-DG anchors α-DG to the cell membrane, and the cytoplasmic domain of β-DG interacts with dystrophin, which binds to F-actin (Jung *et al.* 1995).

Dystroglycan is also expressed in various non-muscle tissues including peripheral nerve. DG is expressed in Schwann cells, where it localizes to the outer membrane apposing the basal lamina (Saito *et al.* 1999) and the microvilli at the nodal axoglial interface (Saito *et al.* 2003). The Schwann cell DG interacts with laminin and agrin (Yamada *et al.* 1996; Previtali *et al.* 2003) and forms a

Received August 9, 2006; revised manuscript received December 19, 2006; accepted December 27, 2006.

Address correspondence and reprint requests to Kiichiro Matsumura, Department of Neurology and Neuroscience, Teikyo University, Tokyo 173-8605, Japan. E-mail: k-matsu@med.teikyo-u.ac.jp

Abbreviations used: AChE, acetylcholinesterase; AChR, acetylcholine receptor; DG, dystroglycan; DGC, dystrophin-glycoprotein complex; ECM, extracellular matrix; FCMD, Fukuyama-type congenital muscular dystrophy; NMJ, neuromuscular junction; α-BTX, α-bungarotoxin.

DGC-like complex with Dp116, utrophin, sarcoglycans, dystrophin-related protein 2 (DRP2) and L-periaxin (Saito *et al.* 1999; Imamura *et al.* 2000; Sherman *et al.* 2001). We have previously demonstrated that Schwann cell DG is necessary for myelination of peripheral nerve (Saito *et al.* 2003).

Recently, primary mutations of the genes encoding known or putative glycosyltransferases have been identified in several forms of congenital muscular dystrophies, which are characterized by muscular dystrophy with onset during the neonatal period accompanied by variable brain and ocular anomalies (Muntoni *et al.* 2004). In these diseases, laminin-binding activity of α-DG has been shown to be greatly reduced in skeletal muscle because of aberrant glycosylation of α-DG (Michele *et al.* 2002), and they are now correctively called α-dystroglycanopathy (Toda *et al.* 2003). Among them, Fukuyama-type congenital muscular dystrophy (FCMD), which is caused by the mutation of the *fukutin* gene, is one of the most common autosomal recessive disorders in Japan (Kobayashi *et al.* 1998). Fukutin is a ubiquitously expressed Goldi-resident protein shearing homology with fringe-like glycosyltransferases (Aravind and Koonin 1999). Because the constitutive fukutin knockout is embryonic lethal in mice, we generated fukutin-deficient chimeric mice and demonstrated that these mice developed severe muscular dystrophy, brain anomaly and eye abnormality (Takeda *et al.* 2003; Chiyonobu *et al.* 2005; Kurahashi *et al.* 2005).

Although involvement of the peripheral nervous system has not been characterized in FCMD so far, it is intriguing to hypothesize that the deficiency of fukutin may cause abnormal myelination of peripheral nerve because of aberrant glycosylation of Schwann cell α-DG. In addition, α-DG is a receptor for agrin, a potent regulator of acetylcholine receptor (AChR) clustering at the post-synaptic membrane of neuromuscular junction (NMJ) (Bowe *et al.* 1994). Several lines of evidence have implicated DG in the formation and maintenance of NMJ (Cote *et al.* 1999; Peng *et al.* 1999; Grady *et al.* 2000; Jacobson *et al.* 2001). These observations prompted us to hypothesize that the clustering of AChR at NMJ may be altered in α-dystroglycanopathy. To test this possibility, we investigated the status of myelination of peripheral nerve and clustering of AChR at NMJ in the fukutin-deficient chimeric mice.

Materials and methods

Generation of fukutin-deficient chimeric mice

The design of the fukutin targeting construct and generation of fukutin-deficient chimeric mice were reported previously (Takeda *et al.* 2003). We used mice with more than 80% contribution of fukutin$^{-/-}$ cells judged by chimerism of coat color as fukutin-deficient chimeric mice and those with 0% contribution as their control.

Antibodies

Rabbit polyclonal antibody against 34 amino acids in the C-terminal domain of human α-DG (DKGGLSAVDAFEIHVHRRPQGDRAPARFKAKFVG) was generated and affinity purified (AP1530). Mouse monoclonal antibody IIH6 against sugar chain of α-DG and 8D5 against C-terminal domain of β-DG were kindly gifted by Dr K. P. Campbell (University of Iowa) and the late Dr L. V. B. Anderson (Newcastle General Hospital), respectively. Mouse monoclonal antibody 2D9 against laminin α2 chain was kindly provided by Dr H. Hori (Tokyo Medical and Dental University). Mouse monoclonal antibody against C-terminal end of dystrophin (MANDRA 1) and affinity isolated rabbit anti-laminin were obtained from Sigma (St. Louis, MO, USA). Rabbit polyclonal antibody against synaptophysin and mouse monoclonal anti-dystrobrevin was purchased from Novocastra and BD Biosciences (San Jose, CA, USA), respectively. Mouse monoclonal antibodies against agrin, laminin β1 and β1-integrin (clone MB1.2) were from Chemicon (Temecula, CA, USA). Mouse monoclonal anti-laminin γ1 antibody was purchased from Santa Cruz (Santa Cruz, CA, USA). FITC- or Cy3-conjugated secondary antibodies were obtained from the Jackson laboratory (Bar Harbor, ME, USA) and horseradish peroxidase-labeled secondary antibodies were obtained from Roche (Basel, Switzerland).

Histopathological, immunohistochemical and electron microscopic analyses

Histopathological analysis was performed on the fukutin-deficient chimeric mice and age matched control mice between the ages of post-natal day 15 and 24 months using standard frozen section, epon section, and electron microscopic techniques. Immunofluorescent microscopic analysis of peripheral nerve and skeletal muscle was performed as described previously (Michele *et al.* 2002). To obtain longitudinal images of NMJs, sternocleidomastoid muscle was fixed in 1% paraformaldehyde in PBS for 20 min and incubated with 30% sucrose overnight. Then, the specimens were cryosectioned at 40 μm thickness, immunostained and observed using LSM310 confocal microscope (Zeiss, Carl Zeiss, Göttingen, Germany). For the detection of NMJs, tetramethylrhodamine-labeled α-bungarotoxin (BTX), Alexa fluor 488-labeled α-BTX (Invitrogen-Molecular Probes, Carlsbad, CA, USA) or FITC-labeled fasciculin 2 was employed. Fasciculin 2 (Sigma) was labeled with FITC using Fluoreporter FITC protein labeling kit (Molecular Probe) according to the protocol provided by the manufacturer. The density of myelinated nerve fibers was calculated by counting the number of myelinated fibers in a spinal root and dividing the number by the area, using ImageJ software (NIH, Bethesda, MD, USA). The density was calculated in 10 roots and the statistical difference was evaluated by *t*-test.

In situ ligand overlay assay

Recombinant rat C-terminal agrin (R & D Systems, Minneapolis, MN, USA) or mouse EHS laminin (Biomedical Technologies Inc., Stoughton, MA, USA) was labeled with FITC using Fluoreporter FITC protein labeling kit (Invitrogen-Molecular Probe). Frozen quadriceps muscle of fukutin-deficient chimeric mice and control mice was cryosectioned at 8 μm thickness. After blocking with 3% BSA in buffer A (10 mmol/L triethanolamine, pH 7.6, 140 mmol/L NaCl, 1 mmol/L $CaCl_2$, 1 mmol/L $MgCl_2$), the cross sections were

overlaid with FITC-labeled agrin or laminin in buffer A for 3 h. Later the specimen were washed with buffer A and observed using immunofluorescent microscope (Carl Zeiss). In some experiments, they were double stained with tetramethylrhodamine-labeled α-BTX.

Immunoblotting, blot overlay and solid-phase binding assays

For biochemical analysis, tissues were isolated and disrupted using Polytron (Kinematica, Littau-Lucerne, Switzerland) followed by Dounce homogenization in 50 mmol/L Tris–HCl, pH 7.4, 150 mmol/L NaCl, 0.6 μg/mL pepstatin A, 0.5 μg/mL leupeptin, 0.5 μg/mL aprotinin, 0.75 mmol/L benzamidine, and 0.1 mmol/L PMSF. After briefly spinning down debris, the homogenate was applied to 3–12% SDS-PAGE and resolved under reducing condition. Immunoblot analysis was performed as described previously (Michele *et al.* 2002). Blot overlay assay was performed as described previously (Michele *et al.* 2002), using EHS laminin, human merosin (laminin-2) (Chemicon) and recombinant rat C-terminal agrin as probes. Anti-agrin antibody (Chemicon) was used to detect the bound agrin. Solid-phase binding assay was performed as previously described (Michele *et al.* 2002).

Results

Myelination of peripheral nerve is defective in fukutin-deficient chimeric mice

To see if the deficiency of fukutin affects peripheral nerve architecture, we evaluated cross sections from various nerves of fukutin-deficient chimeric mice using light microscope. In the chimeric spinal roots, sciatic nerves and tibial nerves from post-natal day 15 (P15) to 23 months of age, the density of myelinated nerve fibers was decreased compared with control (Figs 1a and b). Morphometric quantification confirmed significant reduction of myelinated fiber density in the chimeric mice (Fig. 1c). Remarkably, in the spinal roots and sciatic nerves of P30 chimeric mice, there were numerous abnormally pale-staining areas, which consisted of clusters of densely packed non-myelinated axons (Figs 1d and e). Moreover, in the spinal roots of the old chimeric mice (>20 months old), nerve bundles in which myelinated fibers were strikingly decreased or lost were occasionally observed (Figs 1f and g).

We performed electron microscopic analysis of peripheral nerve of the chimeric mice. Because the aforementioned morphological abnormalities were most prominent in the spinal roots of old chimeric mice, we analyzed the chimeric mice of 20–23 months of age. In the spinal roots of the chimeric mice, non-myelinated axons with abnormally large caliber were frequently observed (Fig. 2a). Typically, these non-myelinated axons were larger than 1 μm in diameter and surrounded by much smaller non-myelinated axons. In many cases, ensheathment of these abnormally large non-myelinated axons was incomplete and their cytoskeletal structures were obscure, indicating they were degenerated (Fig. 2a). Occasionally, Schwann cells that appeared to ensheath multiple myelinated axons were observed (Fig. 2b). In the nerve bundles where severe decrement of myelinated fibers was observed under light microscope (Figs 1f and g), Schwann cells surrounding numerous degenerated axons with or without myelin or myelin ovoids were found (Fig. 2c). Many non-myelinated axons were very large in diameter and their cytoskeletal structures were obscure (Fig. 2c). In the Schwann cell cytoplasm, numerous degradated mitochondria and other cell organelles were accumulated (Fig. 2c). On the other hand, the outer membrane of Schwann cells in these degenerated nerve bundles were normally surrounded by typical mature basal lamina (Fig. 2d).

Aberrant glycosylation and reduced laminin-binding activity of α-DG in the peripheral nerve of fukutin-deficient chimeric mice

To see if the deficiency of fukutin affects the expression of the components of the DGC in peripheral nerve, we examined the sciatic nerve of fukutin-deficient chimeric mice by immunofluorescent microscope. The immunoreactivity of α-DG revealed by antibody against sugar chain moiety of α-DG (IIH6) was localized to the outermost layer of myelin sheath in the control mice, whereas the signal was severely decreased in the chimeric mice (Fig. 3). In sharp contrast, the immunoreactivity of α-DG revealed by antibody against core protein of α-DG (AP1530) was localized to the outermost layer of myelin sheath in both control and chimeric mice, and was indistinguishable between them (Fig. 3). Other components of the DGC, including β-DG, utrophin, dystrobrevin, and ECM proteins, such as laminin α2, β1 and γ1 chains were all localized to the outer membrane of myelin sheath or endoneurial basal lamina in both control and chimeric mice, and their expression was indistinguishable between them (Fig. 3).

Consistent with these results, immunoblotting with antibody against sugar chain moiety of α-DG (IIH6) revealed severe reduction of immunoreactivity of 120 kD α-DG in the chimeric sciatic nerve compared with control (Fig. 4a). In contrast, antibody against core protein of α-DG (AP1530) demonstrated only slight reduction of 120 kD α-DG in the chimeric sciatic nerve (Fig. 4a). Interestingly, this antibody detected an additional band of 80 kD, suggesting that considerable portion of α-DG might be aberrantly hypoglycosylated and migrate faster in the chimeric sciatic nerve (Fig. 4a, arrowhead). On the other hand, the expression of β-DG, laminin β1, γ1 chain and Dp116, a Schwann cell specific isoform of dystrophin, was indistinguishable between the control and chimeric mice (Fig. 4a). As sugar chain structure of α-DG plays an essential role in the binding of laminin, we assessed the laminin-binding activity of α-DG in sciatic nerve. Blot overlay assay demonstrated that the binding of laminin-2 to α-DG was greatly reduced in the chimeric sciatic nerve (Fig. 4b). To further confirm the reduction of laminin-binding activity in the chimeric sciatic

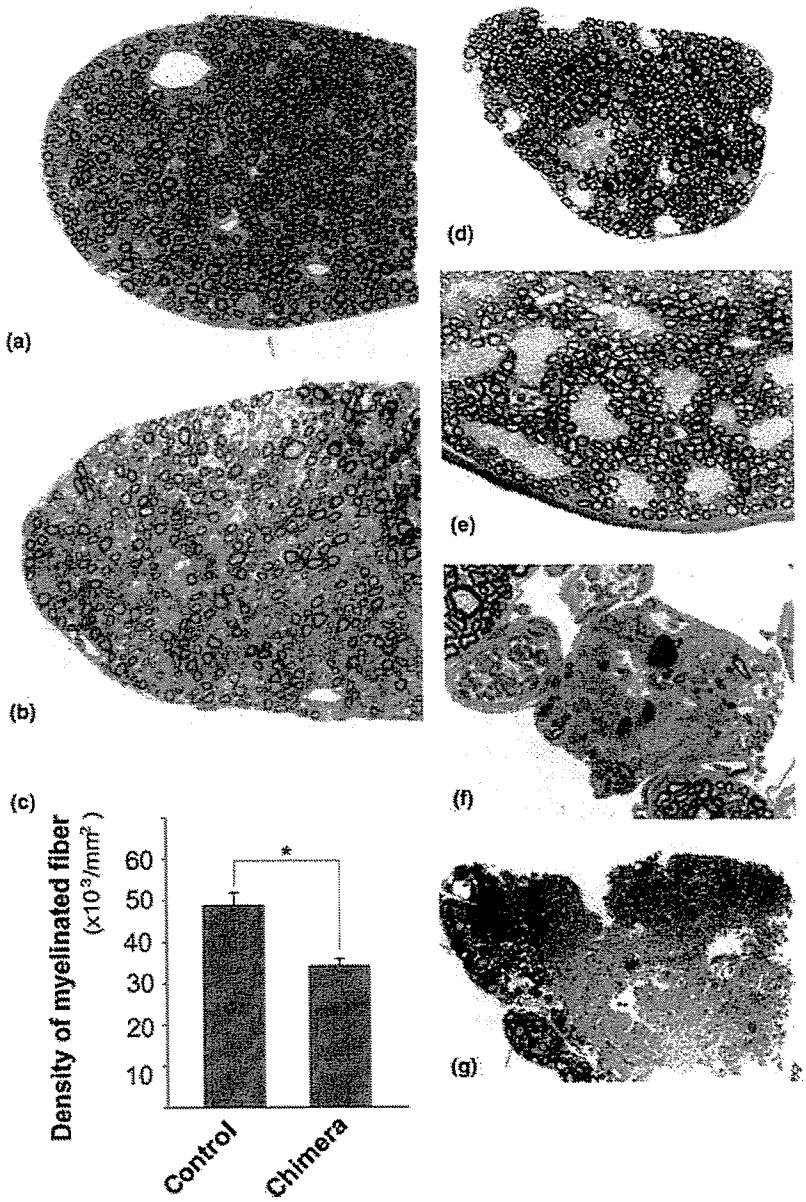

Fig. 1 Defects of myelin formation and radial sorting of axons in the peripheral nerve of fukutin-deficient chimeric mice. (a and b) Toluidine blue-stained epon sections of spinal roots from the post-natal day 15 (P15) control (a) and chimeric mice (b). In the chimeric nerves, the density of myelinated nerve fibers was decreased compared with control. (c) Morphometric quantification revealed significant reduction of myelinated fiber density in the spinal roots of P15 chimeric mice. (d and e) In the roots and sciatic nerves of P30 chimeric mice, there were numerous abnormally pale-staining areas, which were clusters of densely packed non-myelinated axons. (f and g) In the spinal roots of old chimeric mice, nerve bundles in which myelinated fibers were strikingly decreased or lost, were occasionally observed. (f) 20-month old mouse; (g) 23-month old mouse.

nerve, we performed quantitative solid-phase assay. The total laminin-binding activity of chimeric sciatic nerve was decreased to 20% of control (Fig. 4b).

Preservation of β1-integrin in the peripheral nerve of fukutin-deficient chimeric mice

We also analyzed the expression of β1-integrin, which has been shown to play a role in peripheral myelination (Feltri *et al.* 2002). Immunohistochemical analysis revealed that β1-integrin was equally localized to the outermost layer of myelin sheath in both control and chimeric mice (Fig. 5a). Immunoblot analysis also confirmed that the expression of β1-integrin was indistinguishable between the control and chimeric mice (Fig. 5b).

Architecture of neuromuscular junction is defective in fukutin-deficient chimeric mice

To evaluate AChR clustering, quadriceps muscle was stained with Alexa fluor 488-labeled α-bungarotoxin (α-BTX), a specific marker for AChR. Interestingly, NMJs of the chimeric mice were much smaller than control (Fig. 6a). We also analyzed the *en face* topology of NMJ labeled with α-BTX in longitudinal sections of sternocleidomastoid muscle. In the control mice, the pattern of AChR staining was smooth and continuous in appearance (Fig. 6b). On the other hand, NMJs of the chimeric mice showed a fragmented and discontinuous pattern of AChR staining defined by some discrete cups (Fig. 6b).

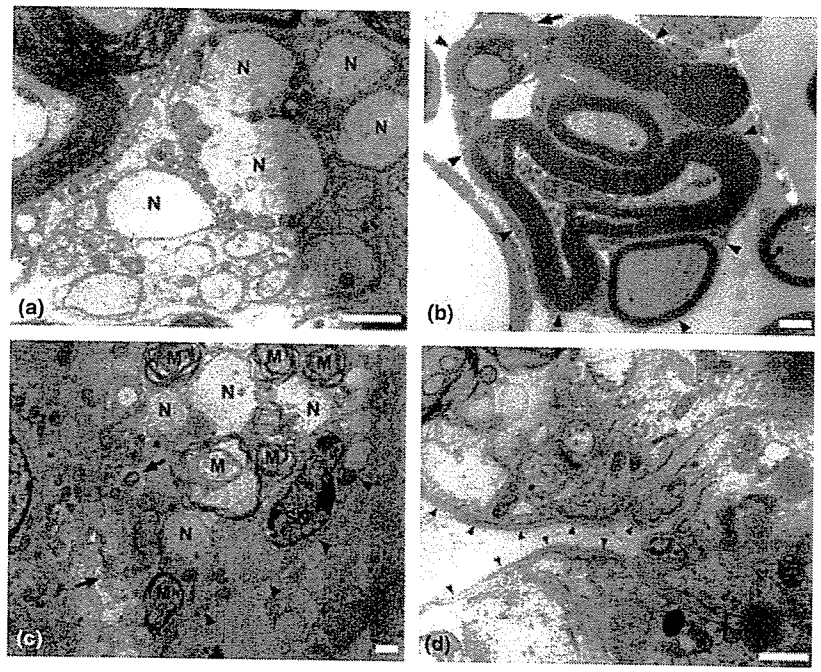

Fig. 2 Ultrastructural abnormalities of peripheral nerve in fukutin-deficient chimeric mice. Electron microscopic analysis of the spinal roots was performed using chimeric mice of 20 (a, c, d) and 23 (b) months of age. (a) Non-myelinated axons with abnormally large caliber were frequently observed. They were surrounded by much smaller non-myelinated axons. Ensheathment of these abnormally large non-myelinated axons was incomplete and their cytoskeletal structures were obscure, indicating that they were degenerated. N: degenerated large non-myelinated axons. (b) A single Schwann cell appeared to ensheath multiple myelinated axons and a non-myelinated axon (arrow). Arrowheads indicate the outer membrane of a Schwann cell. (c) Schwann cells surrounded many degenerated axons with or without myelin or myelin ovoids. Many of the non-myelinated axons were very large in diameter and cytoskeletal structures inside of the axons were obscure. In the Schwann cell cytoplasm, numerous degradated mitochondria and other cell organelles were accumulated (arrow). M: degenerated myelinated axons or myelin ovoid, N: degenerated abnormally large non-myelinated axons, SN: Schwann cell nuclei. Arrowheads indicate the outer membrane of a Schwann cell. (d) The Schwann cell outer membrane of degenerated nerve bundles was normally surrounded by mature basal lamina (arrowhead). Scale bar indicates 1 μm.

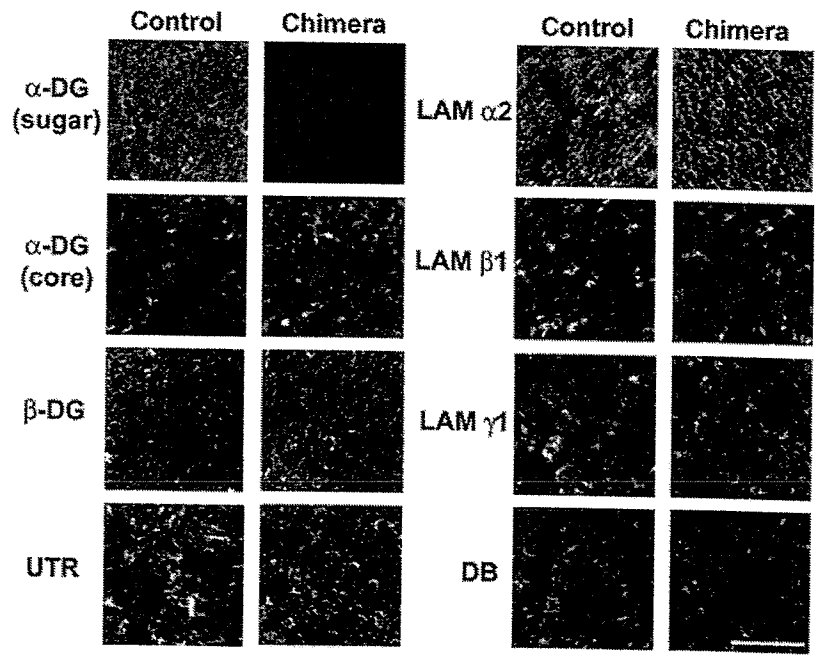

Fig. 3 Abnormal expression of α-DG in the peripheral nerve of fukutin-deficient chimeric mice. Immunohistochemical analysis revealed that the immunoreactivity for sugar chain moiety of α-DG recognized by monoclonal antibody IIH6 was localized to the outermost layer of myelin sheath in the control sciatic nerve, whereas the signal was severely decreased in the chimeric sciatic nerve. In contrast, the immunoreactivity of α-DG revealed by antibody against its core protein (AP1530) was localized to the outermost layer of myelin sheath in both control and chimeric mice, and was indistinguishable between them. β-DG, utrophin, dystrobrevin, laminin α2, β1 or γ1 were normally expressed at the outer membrane of myelin sheath or endoneurial basal lamina in both control and chimeric sciatic nerves. UTR, utrophin; LAM, laminin; DB, dystrobrevin. Scale bar indicates 50 μm.

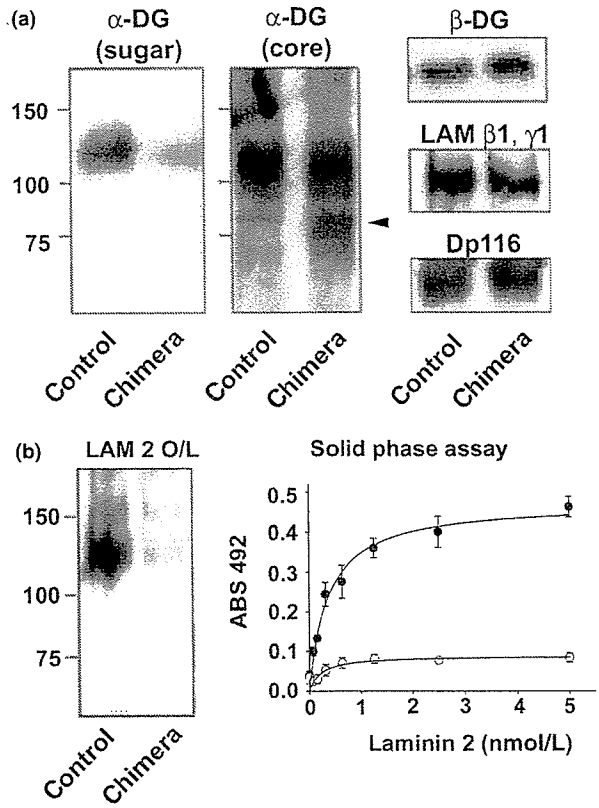

Fig. 4 Hypoglycosylation and reduced laminin-binding activity of α-DG in the peripheral nerve of fukutin-deficient chimeric mice. (a) Immunoblot analysis revealed severe reduction of immunoreactivity of 120 kD α-DG in the chimeric sciatic nerve when probed with IIH6, an antibody against sugar chain moiety of α-DG. In contrast, antibody against core protein of α-DG demonstrated only slight reduction of 120 kD α-DG in the chimeric sciatic nerve. Interestingly, an additional band of 80 kD was observed (arrowhead), suggesting that considerable fraction of α-DG was hypoglycosylated in the chimeric sciatic nerve. The expression of β-DG, laminin β1, γ1 or Dp116 was not altered. (b) Blot overlay assay demonstrated that the binding activity of α-DG to laminin-2 was greatly reduced in the chimeric sciatic nerve (left). Solid-phase binding assay demonstrated that the binding activity of α-DG to laminin-2 was quantitatively decreased in the chimeric sciatic nerve (right). LAM, laminin; O/L, overlay assay.

To see if the deficiency of fukutin affects the expression of α-DG at NMJ, we performed double immunostaining analysis using antibodies against α-DG. The immunoreactivity of α-DG with antibody against core protein of α-DG (AP1530) was localized to the NMJ as well as extrajunctional sarcolemma in both control and chimeric mice (Fig. 6a). When α-DG was probed with antibody against sugar chain moiety of α-DG (IIH6), the immunostaining of the NMJ as well as extrajunctional sarcolemma was severely reduced in the chimeric mice, indicating aberrant glycosylation of α-DG not only at the extrajunctional sarcolemma but also NMJ (Fig. 6a).

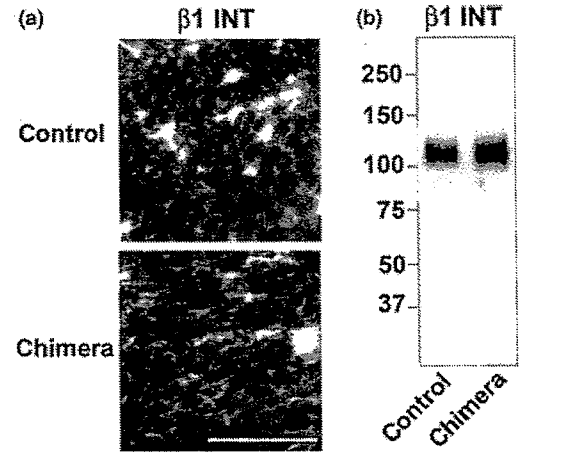

Fig. 5 Preservation of β1-integrin in the peripheral nerve of fukutin-deficient chimeric mice. Immunohistochemical analysis revealed that β1-integrin was equally localized to the outermost layer of myelin sheath in both control and chimeric mice (a). Immunoblot analysis confirmed that the expression of β1-integrin was indistinguishable between the control and chimeric mice (b). Scale bar indicates 50 μm. INT, integrin.

Quadriceps muscle was double-stained with α-BTX and fasciculin 2, which specifically labels acetylcholinesterase (AChE) (Peng *et al.* 1999). In the control mice, the labeling with fasciculin 2 was co-localized with α-BTX at the NMJ (Fig. 7a). In the chimeric mice, in contrast, the fasciculin 2 staining of NMJ was much smaller than control, although it was co-localized with α-BTX (Fig. 7a). Quadriceps muscle was also double-stained with α-BTX and antibody against synaptophysin, a marker for pre-synaptic nerve terminal. In the control mice, the immunoreactivity of synaptophysin was co-localized with α-BTX at the NMJ (Fig. 7b). In the chimeric mice, in contrast, the synaptophysin staining of NMJ was much smaller than control, although it was co-localized with α-BTX (Fig. 7b).

Agrin is not stably expressed and agrin-binding activity of α-DG is decreased at the neuromuscular junction in fukutin-deficient chimeric mice

To investigate the mechanism of defective NMJ formation in the fukutin-deficient chimeric mice, we assessed the expression of agrin, a key molecule involved in the clustering of AChR. Immunofluorescent analysis demonstrated that agrin was expressed at the sarcolemma in the control mice, whereas its expression was significantly reduced in the chimeric mice (Fig. 8). Furthermore, agrin was enriched at the NMJ in the control mice, where it was co-localized with AChR as probed by α-BTX (Fig. 8). In sharp contrast, agrin was not clearly detected at the NMJ in the chimeric mice (Fig. 8). Apart from agrin, laminin has also been implicated in the clustering of AChR at the NMJ (Sugiyama *et al.* 1997). Therefore, we studied the expression of laminin at the

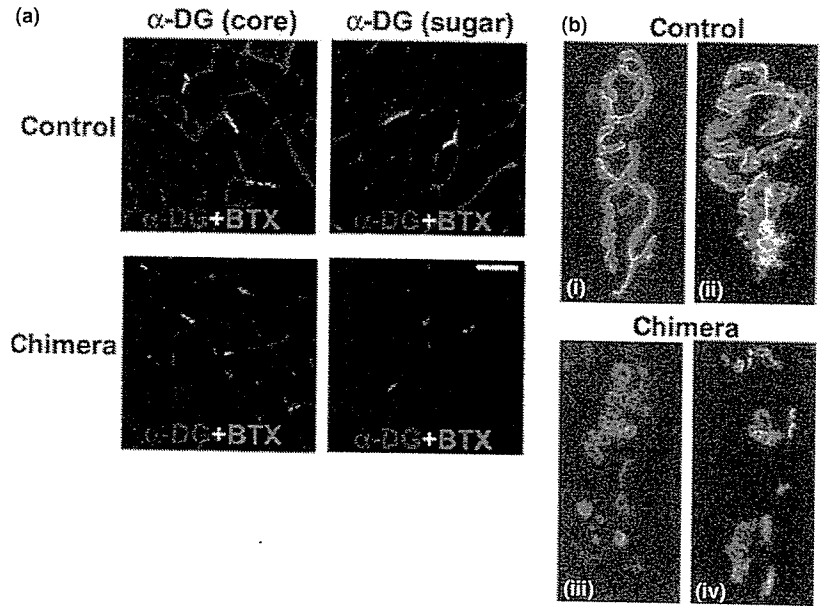

Fig. 6 Small and fragmented neuromuscular junctions (NMJ) in fukutin-deficient chimeric mice. (a) Double staining of quadriceps muscle with anti-α-DG core protein (red) and Alexa fluor 488-labeled α-BTX (green). Chimeric NMJs were small and fragmented in appearance compared with control. When α-DG was probed with antibody against sugar chain moiety of α-DG (IIH6), immunostaining of the NMJ as well as extrajunctional sarcolemma was severely reduced in the chimeric mice. Scale bar indicates 50 μm. (b) Longitudinal sections of sternocleidomastoid muscle stained by α-BTX. In the control mice, the pattern of AChR staining was smooth and continuous in appearance. In contrast, NMJs of the chimeric mice showed a discontinuous and fragmented pattern of AChR staining. Scale bar indicates 10 μm.

sarcolemma and NMJ. Although laminin was localized to the NMJ as well as extrajunctional sarcolemma in the control mice, its expression was severely reduced in these locations in the chimeric mice.

Next, we evaluated the agrin and laminin-binding activity of α-DG at the NMJ. First, we overlaid the blots of the total homogenate of skeletal muscle with agrin or laminin. The binding of both agrin and laminin to α-DG was greatly reduced in the chimeric mice compared with control (Figs 9a and b, left panels). Then, to assess the agrin and laminin-binding activity of α-DG at the NMJ and extrajunctional sarcolemma separately, we performed *in situ* ligand overlay assay. The cross sections of skeletal muscle were overlaid with extrinsic agrin or laminin labeled by FITC. The FITC-labeled agrin bound to both NMJ and extrajunctional sarcolemma in the control skeletal muscle (Fig. 9a, right panel). The binding of agrin was stronger at the NMJ than extrajunctional sarcolemma as revealed by double staining with α-BTX (Fig. 9a, right panel). In sharp contrast, agrin bound only weakly to the NMJ and did not significantly bind to the extrajunctional sarcolemma in the chimeric mice (Fig. 9a, right panel). We also performed *in situ* laminin overlay assay. When the skeletal muscle was overlaid with FITC-labeled extrinsic laminin, laminin bound strongly to the NMJ as well as extrajunctional sarcolemma in the control mice (Fig. 9b, right panel). However, laminin did not significantly bound to the NMJ or extrajunctional sarcolemma in the chimeric mice (Fig. 9b, right panel).

Discussion

In the present study, we have shown the decreased density of myelinated nerve fibers in the peripheral nerve of fukutin-deficient chimeric mice. This was observed from P15 to 23 months of age. By electron microscopy, numerous non-myelinated axons with abnormally large caliber were observed. These large non-myelinated axons were surrounded by small calibered non-myelinated axons and ensheathed by the same Schwann cell. During the normal development of peripheral nerve, individual Schwann cells either ensheath multiple small non-myelinated axons or sort larger axons into 1 : 1 relationship, forming a myelinated axon. Typically, axons with a diameter of 1 μm or greater are myelinated (Peters *et al.* 1991). In our chimeric mice, however, many axons larger than 1 μm in diameter were left unmyelinated and ensheathed together with much smaller axons by the same Schwann cell. These findings indicate that the radial sorting mechanism is defective in the chimeric mice. In support of this notion, Schwann cells that appeared to ensheath multiple myelinated axons were also observed. In the spinal roots and sciatic nerves of young chimeric mice (P30), furthermore, large clusters of non-myelinating Schwann cells were observed.

These findings resembled those reported in *dystrophic mice* (dy/dy, dy^{2j}/dy^{2j}), which have mutations in the gene encoding laminin α2 chain (Sunada *et al.* 1995). The defective myelin formation in these mice is characterized by the clusters of juxtaposed non-myelinated axons, which are most prominent in the nerve roots (Bradley and Jenkison 1973). Similar clusters of non-myelinated axons were also observed in the mice with targeted disruption of laminin γ1 or laminin α4 chain (Chen and Strickland 2003; Wallquist *et al.* 2005; Yang *et al.* 2005). Interestingly, myodystrophic mice (*myd*) and enervated mice (*enr*), in which mutations of the *Large* gene result in the reduction of laminin-binding activity of skeletal muscle α–DG, exhibit similar defects in

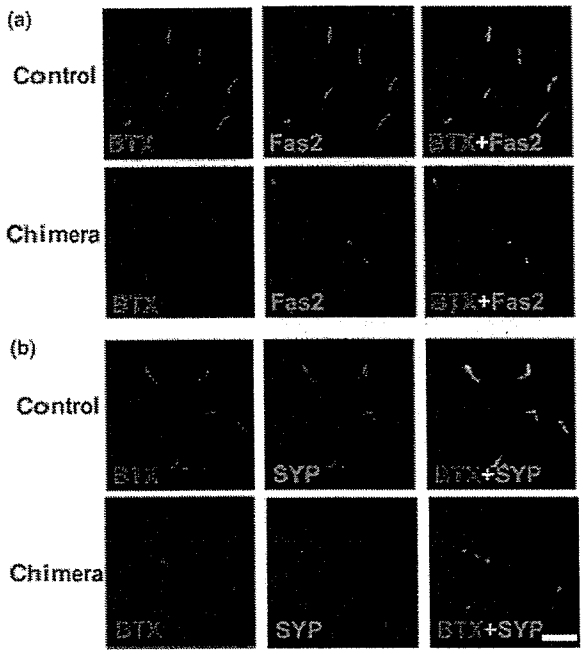

Fig. 7 Defective expression of acetylcholinesterase and synaptophysin at the neuromuscular junction (NMJ) of fukutin-deficient chimeric mice. (a) Quadriceps muscle was double-stained with rhodamine-labeled α-BTX (red) and FITC-labeled fasciculin 2 (green), a marker for AChE. In the control mice, the labeling with fasciculin 2 was co-localized with AChR. In the chimeric mice, the labeling with fasciculin 2 was much smaller than control, although it was co-localized with α-BTX staining. (b) Quadriceps muscle was double-stained with rhodamine-labeled α-BTX (red) and antibody against synaptophysin (green), a marker for presynaptic nerve terminal. Although the immunoreactivity of synaptophysin was co-localized with AChR in both control and chimeric mice, the staining was much smaller in the chimeric than control mice. BTX, bungarotoxin; Fas2, fasciculin 2; SYP, synaptophysin. Scale bar indicates 50 μm.

radial sorting (Rayburn and Peterson 1978; Kelly *et al.* 1994; Levedakou *et al.* 2005).

In the present study, we have found that the sugar chain moiety and laminin-binding activity of α–DG were severely reduced in the peripheral nerve of fukutin-deficient chimeric mice, suggesting that hypoglycosylation of α–DG might play a role in the pathogenesis of the aforementioned phenotype of the chimeric mice. We have previously demonstrated that the selective disruption of the DG gene in Schwann cells results in defective myelination in mice (P0-DG null mice). However, the hallmarks of the pathological findings of these mice were somewhat different from those of the fukutin-deficient chimeric mice, and irregular thickening and extensive folding of myelin sheath of peripheral nerve fibers were the major findings (Saito *et al.* 2003). Interestingly, in this respect, it was proposed that substrates of Large in addition to α–DG might be involved in the pathogenesis of the phenotype of *myd* and *enr* mice (Levedakou and Popko 2006). At present, target glycoproteins of fukutin, Large and related glycosyltransferases remain unidentified except α-DG. Under these circumstances, we analyzed the expression of β1-integrin in the chimeric sciatic nerve, because (1) its ablation has been shown to result in the formation of bundles of non-myelinated axons (Feltri *et al.* 2002) and (2) there is a possibility that β1-integrin, which is a glycoprotein, could be a target of fukutin and related glycosyltransferases. However, we did not find a significant abnormality in its expression, suggesting that dysfunction of β1-integrin may not play a significant role in the pathogenesis of impaired radial sorting of axons in the fukutin-deficient chimeric mice.

Recently, mutations of the gene encoding L-periaxin, a Schwann cell cytoplasmic protein that interacts with β-DG via DRP2, were identified in Charcot-Marie-Tooth disease type 4F (Boerkoel *et al.* 2001; Sherman *et al.* 2001).

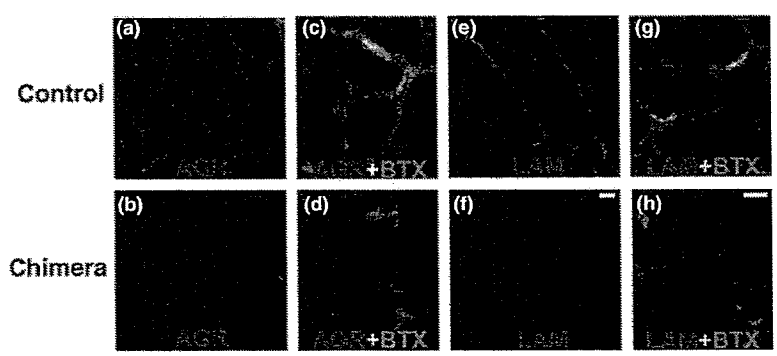

Fig. 8 Decreased expression of agrin and laminin at the neuromuscular junction (NMJ) in fukutin-deficient chimeric mice. Immunohistochemical analysis demonstrated that agrin (red) was expressed in the sarcolemma in the control mice (a), whereas its expression was significantly reduced in the chimeric mice (b). Agrin was enriched at the NMJ of the control mice where it was co-localized with AChR probed by FITC-labeled α-BTX (green) (c). In contrast, agrin was severely reduced in the sarcolemma and not clearly detected at the NMJ in the chimeric mice (d). Laminin α2 (red) was localized to the NMJ as well as extrajunctional sarcolemma in the control mice (e, g). However, its expression was severely reduced at both NMJ and extrajunctional sarcolemma in the chimeric mice (f, h). AGR, agrin; BTX, bungarotoxin; LAM, laminin α2. Scale bar indicates 20 μm.

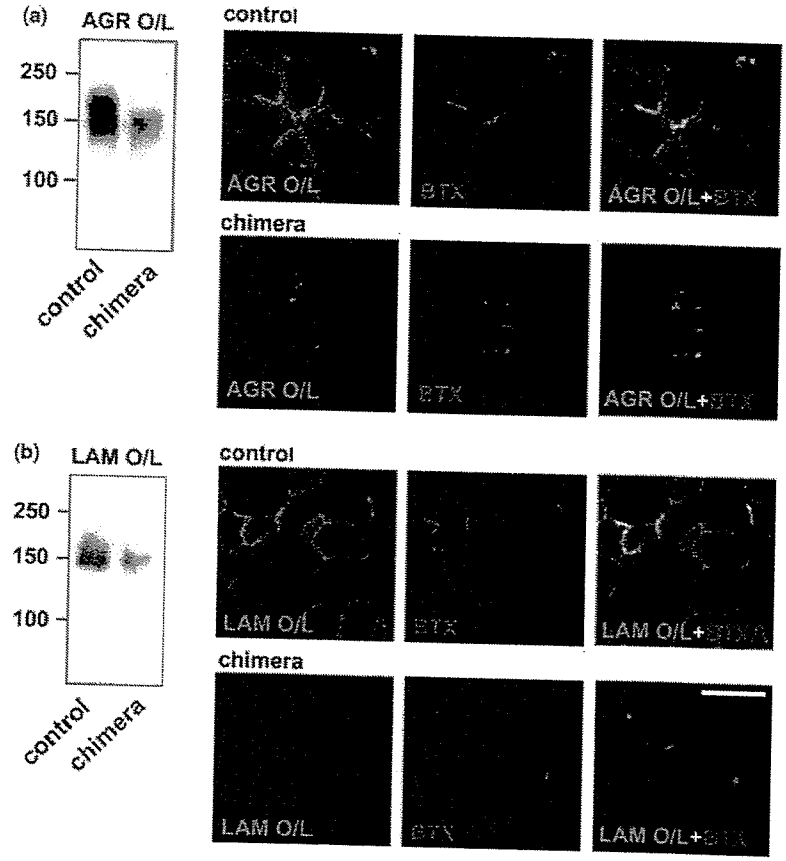

Fig. 9 Decreased ligand-binding activity of α-DG at the neuromuscular junction (NMJ) of fukutin-deficient chimeric mice. (a) Blot overlay assay demonstrated that the binding activity of α-DG to agrin was reduced in the skeletal muscle of chimeric mice (left). *In situ* ligand binding assay showed that FITC-labeled agrin (green) bound to both NMJ and extrajunctional sarcolemma in the control mice. The binding of agrin was stronger at the NMJ than extrajunctional sarcolemma as revealed by double staining with rhodamine-labeled α-BTX (red). In sharp contrast, agrin bound only weakly to the NMJ and did not bind significantly to the extrajunctional sarcolemma in the chimeric mice (right). (b) Blot overlay assay revealed that the binding activity of α-DG to laminin was reduced in the skeletal muscle of chimeric mice (left). FITC-labeled laminin bound strongly to the NMJ as well as extrajunctional sarcolemma in the control mice. However, laminin did not bind to the NMJ or extrajunctional sarcolemma in the chimeric mice (right). AGR, agrin; BTX, bungarotoxin; LAM, laminin; O/L, overlay assay. Scale bar indicates 50 μm.

Peripheral nerve of the patients and its mouse model exhibited hypermyelination and in/out-folding of myelin sheath as well as demyelination/remyelination, which were very similar to those observed in the P0-DG null mice (Gillespie *et al.* 2000; Boerkoel *et al.* 2001; Guilbot *et al.* 2001). Taken together, it would be intriguing to postulate that disruption of the extracellular linkage of DG may lead to the impaired radial sorting of axons, while disruption of the cytoplasmic linkage of DG may result in extensive myelin folding or hypermyelination. The other intriguing possibility would be that glycoconjugates other than α-DG and β1-integrin might be hypoglycosylated in the fukutin-deficient chimeric mice and that this might lead to the impaired radial sorting of axons.

In addition to the impaired radial sorting, degradation of cytoskeletal structure and cell organelles was observed in the axon and Schwann cell cytoplasm in the older chimeric mice. These observations suggest that impairment of radial sorting which occurred during the late embryonic to early post-natal stages may eventually lead to degeneration of these cells and result in the formation of abnormal nerve bundles seen in the old chimeric mice over a long period of time.

In the fukutin-deficient chimeric mice, the architecture of NMJ was abnormal. The NMJs were fragmented in appearance and the normal continuous pattern of AChR staining was lost. These observations are consistent with our recent report of aberrant NMJ in the patients with FCMD and *myd* mice (Taniguchi *et al.* 2006). In the formation of NMJ, agrin derived from motoneurons plays a crucial role in the clustering of AChR at the post-synaptic membrane. The neural agrin activates MuSK, a muscle-specific receptor tyrosin kinase and leads to the clustering of AChR (Sanes *et al.* 1998; Borges and Ferns 2001). α-DG was suggested to be involved in this agrin induced clustering of AChR (Jacobson *et al.* 1998; Kahl and Campanelli 2003). Apart from agrin, laminin also induces the clustering of AChR through a MuSK-independent pathway and DG has been implicated in this process (Sugiyama *et al.* 1997; Montanaro *et al.* 1998; Jacobson *et al.* 2001). Furthermore, DG is also known to mediate the localization of AChE at synaptic basal lamina by interacting with perlecan (Peng *et al.* 1998, 1999). Altogether, these findings suggest that the NMJ fragmentation in the chimeric mice may be caused by disruption of the linkage between α-DG and its ligands, agrin and laminin, because of aberrant glycosylation of α-DG.

To confirm this, we assessed the agrin and laminin-binding activity of α-DG and the expression of agrin and

laminin at the NMJ of the chimeric mice. We found that α-DG was hypoglycosylated at the NMJ of the chimeric mice as revealed by immunohistochemical analysis using antibodies against the core protein (AP1530) and the sugar chain moiety (IIH6) of α-DG. Because several distinct α-DG glycoforms exist in the skeletal muscle and glycosylation of skeletal muscle α-DG is controlled by innervation (Leschziner *et al.* 2000; McDearmon *et al.* 2001), it is also possible that the glycan structures of α-DG at the NMJ may differ from those of extrajunctional sarcolemma. Under these circumstances, it was important to assess the binding activity of α-DG to agrin or laminin at the NMJ exclusively. For this purpose, we performed *in situ* ligand overlay assay using FITC-labeled agrin or laminin. In the control mice, the FITC-labeled extrinsic agrin and laminin bound to the sarcolemma clearly, indicating that the agrin/laminin-binding sugar chain moieties on α-DG are not fully occupied or saturated by the intrinsic agrin/laminin in the basal lamina *in vivo*. Interestingly, the binding of these fluorescent extrinsic ligands to the NMJ and extrajunctional sarcolemma was greatly reduced in the chimeric mice, indicating that the ligand-binding activity of α-DG was defective at the NMJ as well as extrajunctional sarcolemma in the chimeric mice. We also found that the expression of agrin and laninin was decreased at the NMJ and extrajunctional sarcolemma of the chimeric mice. Defective ligand-binding activity of α-DG may explain for the decreased expression of agrin and laninin at the NMJ and extrajunctional sarcolemma of the chimeric mice, because it may destabilize the proper localization of these ligands in the basal lamina. Taken together, our results indicate that disruption of the linkage between α-DG and its ligands leads to the aberrant clustering of AChR at the NMJ. In support of this notion, it was reported recently that the extracellular domain of α-DG modulates agrin-induced AChR aggregation in myotubes (Tremblay and Carbonetto 2006).

We have also found that the expression of synaptophysin, a marker for pre-synaptic nerve terminal, is disturbed at the NMJ in the chimeric mice. At present, we do not have definite explanations for this finding. One possibility is that it may simply reflect the disturbed NMJ formation in the chimeric mice. Another intriguing possibility is that it may be secondary to the defective myelination of peripherall motor nerve fibers in the chimeric mice.

In conclusion, we have demonstrated that fukutin plays a crucial role in the myelination of peripheral nerve and formation of NMJ. We propose that these effects of fukutin are at least partially exerted by regulating the sugar chain structure of α-DG involved in the interaction with laminin and agrin. It would be interesting, in the future, to evaluate the status of peripheral nerve and NMJ in the patients with α-dystroglycanopathies and to clarify the roles of their defects in the expression of the phenotype of theses disorders.

Acknowledgments

We thank Miki Yamanaka and Yuka Sasayama for their expert technical assistance. This work was supported by (1) Research Grants 16B-1 and 17A-10 for Nervous and Mental Disorders (Ministry of Health, Labor and Welfare), (2) Research on Psychiatric and Neurological Diseases and Mental Health (Ministry of Health, Labor and Welfare), and (3) Research Grant 16390256, 40286993, 17590898 and 'Open Research Center' Project for Private Universities: matching fund subsidy from MEXT (Ministry of Education, Culture, Sports, Science and Technology), 2004-2008, (4) The 21st Century COE program from MEXT.

References

Aravind L. and Koonin E. V. (1999) The fukutin protein family–predicted enzymes modifying cell-surface molecules. *Curr. Biol.* **9**, R836–R837.

Boerkoel C. F., Takashima H., Stankiewicz P., Garcia C. A., Leber S. M., Rhee-Morris L. and Lupski J. R. (2001) Periaxin mutations cause recessive Dejerine-Sottas neuropathy. *Am. J. Hum. Genet.* **68**, 325–633.

Borges L. S. and Ferns M. (2001) Agrin-induced phosphorylation of the acetylcholine receptor regulates cytoskeletal anchoring and clustering. *J. Cell Biol.* **153**, 1–12.

Bowe M. A., Deyst K. A., Leszyk J. D. and Fallon J. R. (1994) Identification and purification of an agrin receptor from Torpedo postsynaptic membranes: a heteromeric complex related to the dystroglycans. *Neuron* **12**, 1173–1180.

Bradley W. G. and Jenkison M. (1973) Abnormalities of peripheral nerves in murine muscular dystrophy. *J. Neurol. Sci.* **18**, 227–247.

Chen Z. L. and Strickland S. (2003) Laminin γ1 is critical for Schwann cell differentiation, axon myelination, and regeneration in the peripheral nerve. *J. Cell Biol.* **163**, 889–899.

Chiba A., Matsumura K., Yamada H., Inazu T., Shimizu T., Kusunoki S., Kanazawa I., Kobata A. and Endo T. (1997) Structures of sialylated O-linked oligosaccharides of bovine peripheral nerve α-dystroglycan. *J. Biol. Chem.* **272**, 2156–2162.

Chiyonobu T., Sasaki J., Nagai Y., Takeda S., Funakoshi H., Nakamura T., Sugimoto T. and Toda T. (2005) Effects of fukutin deficiency in the developing mouse brain. *Neuromuscul. Disord.* **15**, 416–426.

Cote P. D., Moukhles H., Lindenbaum M. and Carbonetto S. (1999) Chimaeric mice deficient in dystroglycans develop muscular dystrophy and have disrupted myoneural synapses. *Nat. Genet.* **23**, 338–342.

Ervasti J. M. and Campbell K. P. (1993) A role for the dystrophin-glycoprotein complex as a transmembrane linker between laminin and actin. *J. Cell Biol.* **122**, 809–823.

Feltri M. L., Graus Porta D., Previtali S. C. *et al.* (2002) Conditional disruption of β1-integrin in Schwann cells impedes interactions with axons. *J. Cell Biol.* **156**, 199–209.

Gillespie C. S., Sherman D. L., Fleetwood-Walker S. M. *et al.* (2000) Peripheral demyelination and neuropathic pain behavior in periaxin-deficient mice. *Neuron* **26**, 523–531.

Grady R. M., Zhou H., Cunningham J. M., Henry M. D., Campbell K. P. and Sanes J. R. (2000) Maturation and maintenance of the neuromuscular synapse: genetic evidence for roles of the dystrophin-glycoprotein complex. *Neuron* **25**, 279–293.

Guilbot A., Williams A., Ravise N. *et al.* (2001) A mutation in periaxin is responsible for CMT4F, an autosomal recessive form of Charcot-Marie-Tooth disease. *Hum. Mol. Genet.* **10**, 415–421.

Ibraghimov-Beskrovnaya O., Ervasti J. M., Leveille C. J., Slaughter C. A., Sernett S. W. and Campbell K. P. (1992) Primary structure of dystrophin-associated glycoproteins linking dystrophin to the extracellular matrix. *Nature* **355**, 696–702.

Imamura M., Araishi K., Noguchi S. and Ozawa E. (2000) A sarcoglycan-dystroglycan complex anchors Dp116 and utrophin in the peripheral nervous system. *Hum. Mol. Genet.* **9**, 3091–3100.

Jacobson C., Montanaro F., Lindenbaum M., Carbonetto S. and Ferns M. (1998) α-Dystroglycan functions in acetylcholine receptor aggregation but is not a coreceptor for agrin-MuSK signaling. *J. Neurosci.* **18**, 6340–6348.

Jacobson C., Cote P. D., Rossi S. G., Rotundo R. L. and Carbonetto S. (2001) The dystroglycan complex is necessary for stabilization of acetylcholine receptor clusters at neuromuscular junctions and formation of the synaptic basement membrane. *J. Cell Biol.* **152**, 435–450.

Jung D., Yang B., Meyer J., Chamberlain J. S. and Campbell K. P. (1995) Identification and characterization of the dystrophin anchoring site on β-dystroglycan. *J. Biol. Chem.* **270**, 27 305–27 310.

Kahl J. and Campanelli J. T. (2003) A role for the juxtamembrane domain of β-dystroglycan in agrin-induced acetylcholine receptor clustering. *J. Neurosci.* **23**, 392–402.

Kanagawa M., Saito F., Kunz S. *et al.* (2004) Molecular recognition by LARGE is essential for expression of functional dystroglycan. *Cell* **117**, 953–964.

Kelly D., Chancellor K., Milatovich A., Francke U., Suzuki K. and Popko B. (1994) Autosomal recessive neuromuscular disorder in a transgenic line of mice. *J. Neurosci.* **14**, 198–207.

Kobayashi K., Nakahori Y., Miyake M. *et al.* (1998) An ancient retrotransposal insertion causes Fukuyama-type congenital muscular dystrophy. *Nature* **394**, 388–392.

Kurahashi H., Taniguchi M., Meno C., Taniguchi Y., Takeda S., Horie M., Otani H. and Toda T. (2005) Basement membrane fragility underlies embryonic lethality in *fukutin*-null mice. *Neurobiol. Dis.* **19**, 208–217.

Leschziner A., Moukhles H., Lindenbaum M., Gee S. H., Butterworth J., Campbell K. P. and Carbonetto S. (2000) Neural regulation of α-dystroglycan biosynthesis and glycosylation in skeletal muscle. *J. Neurochem.* **74**, 70–80.

Levedakou E. N. and Popko B. (2006) Rewiring enervated: thinking LARGEr than myodystrophy. *J. Neurosci. Res.* **84**, 237–243.

Levedakou E. N., Chen X. J., Soliven B. and Popko B. (2005) Disruption of the mouse Large gene in the enr and myd mutants results in nerve, muscle, and neuromuscular junction defects. *Mol. Cell Neurosci.* **28**, 757–769.

McDearmon E. L., Combs A. C. and Ervasti J. M. (2001) Differential Vicia villosa agglutinin reactivity identifies three distinct dystroglycan complexes in skeletal muscle. *J. Biol. Chem.* **276**, 35 078–35 086.

Michele D. E., Barresi R., Kanagawa M. *et al.* (2002) Posttranslational disruption of dystroglycan-ligand interactions in congenital muscular dystrophies. *Nature* **418**, 417–422.

Montanaro F., Gee S. H., Jacobson C., Lindenbaum M. H., Froehner S. C. and Carbonetto S. (1998) Laminin and α-dystroglycan mediate acetylcholine receptor aggregation via a MuSK-independent pathway. *J. Neurosci.* **18**, 1250–1260.

Muntoni F., Brockington M., Torelli S. and Brown S. C. (2004) Defective glycosylation in congenital muscular dystrophies. *Curr. Opin. Neurol.* **17**, 205–209.

Peng H. B., Ali A. A., Daggett D. F., Rauvala H., Hassell J. R. and Smalheiser N. R. (1998) The relationship between perlecan and dystroglycan and its implication in the formation of the neuromuscular junction. *Cell Adhes. Commun.* **5**, 475–489.

Peng H. B., Xie H., Rossi S. G. and Rotundo R. L. (1999) Acetylcholinesterase clustering at the neuromuscular junction involves perlecan and dystroglycan. *J. Cell Biol.* **145**, 911–921.

Peters A., Palay S. L. and Webster H. (1991) *The fine structure of the nervous system*, 3rd edn. Oxford Universuty Press, New York.

Previtali S. C., Nodari A., Taveggia C., Pardini C., Dina G., Villa A., Wrabetz L., Quattrini A. and Feltri M. L. (2003) Expression of laminin receptors in schwann cell differentiation: evidence for distinct roles. *J. Neurosci.* **23**, 5520–5530.

Rayburn H. B. and Peterson A. C. (1978) Naked axons in myodystrophic mice. *Brain Res.* **146**, 380–384.

Saito F., Masaki T., Kamakura K., Anderson L. V., Fujita S., Fukuta-Ohi H., Sunada Y., Shimizu T. and Matsumura K. (1999) Characterization of the transmembrane molecular architecture of the dystroglycan complex in Schwann cells. *J. Biol. Chem.* **274**, 8240–8246.

Saito F., Moore S. A., Barresi R. *et al.* (2003) Unique role of dystroglycan in peripheral nerve myelination, nodal structure,and sodium channel stabilization. *Neuron* **38**, 747–758.

Sanes J. R., Apel E. D., Gautam M., Glass D., Grady R. M., Martin P. T., Nichol M. C. and Yancopoulos G. D. (1998) Agrin receptors at the skeletal neuromuscular junction. *Ann. NY Acad. Sci.* **841**, 1–13.

Sherman D. L, Fabrizi C., Gillespie C. S. and Brophy P. J. (2001) Specific disruption of a schwann cell dystrophin-related protein complex in a demyelinating neuropathy. *Neuron* **30**, 677–687.

Sugiyama J. E., Glass D. J., Yancopoulos G. D. and Hall Z. W. (1997) Laminin-induced acetylcholine receptor clustering: an alternative pathway. *J. Cell Biol.* **139**, 181–191.

Sunada Y., Bernier S. M., Utani A., Yamada Y. and Campbell K. P. (1995) Identification of a novel mutant transcript of laminin α 2 chain gene responsible for muscular dystrophy and dysmyelination in dy2 J mice. *Hum. Mol. Genet.* **4**, 1055–1061.

Takeda S., Kondo M., Sasaki J. *et al.* (2003) Fukutin is required for maintenance of muscle integrity, cortical histiogenesis and normal eye development. *Hum. Mol. Genet.* **12**, 1449–1459.

Taniguchi M., Kurahashi H., Noguchi S. *et al.* (2006) Aberrant neuromuscular junctions and delayed terminal muscle fiber maturation in α-dystroglycanopathies. *Hum. Mol. Genet.* **15**, 1279–1289.

Toda T., Kobayashi K., Takeda S. *et al.* (2003) Fukuyama-type congenital muscular dystrophy (FCMD) and α-dystroglycanopathy. *Congenit. Anom.* **43**, 97–104.

Tremblay M. R. and Carbonetto S. (2006) An extracellular pathway for dystroglycan function in acetylcholine receptor aggregation and laminin deposition in skeletal myotubes. *J. Biol. Chem.* **281**, 13 365–13 373.

Wallquist W., Plantman S., Thams S. *et al.* (2005) Impeded interaction between Schwann cells and axons in the absence of laminin α4. *J. Neurosci.* **25**, 3692–3700.

Yamada H., Denzer A. J., Hori H. *et al.* (1996) Dystroglycan is a dual receptor for agrin and laminin-2 in Schwann cell membrane. *J. Biol. Chem.* **271**, 23 418–23 423.

Yang D., Bierman J., Tarumi Y. S. *et al.* (2005) Coordinate control of axon defasciculation and myelination by laminin-2 and -8. *J. Cell Biol.* **168**, 655–666.

PERGAMON

Neuromuscular Disorders 16 (2006) 256–261

www.elsevier.com/locate/nmd

Rapid and accurate diagnosis of facioscapulohumeral muscular dystrophy

Kanako Goto, Ichizo Nishino, Yukiko K. Hayashi *

Department of Neuromuscular Research, National Institute of Neuroscience, National Center of Neurology and Psychiatry (NCNP), 4-1-1 Ogawa-Higashi, Kodaira, Tokyo 187-8502, Japan

Received 10 September 2005; received in revised form 9 January 2006; accepted 18 January 2006

Abstract

Facioscapulohumeral muscular dystrophy (FSHD) is a common muscular disorder, but clinical and genetic complications make its diagnosis difficult. Southern blot analysis detects a smaller sized *Eco*RI fragment on chromosome 4q35 in most facioscapulohumeral muscular dystrophy patients, that contains integral number of 3.3-kb tandem repeats known as D4Z4. The problems for the genetic diagnosis are that southern blotting for facioscapulohumeral muscular dystrophy is quite laborious and time-consuming, and the D4Z4 number is only estimated from the size of the fragment. We developed a more simplified diagnostic method using a long polymerase chain reaction (PCR) amplification technique. Successful amplification was achieved in all facioscapulohumeral muscular dystrophy patients with an *Eco*RI fragment size ranging from 10 to 25 kb, and each patient had a specific polymerase chain reaction product which corresponded to the size calculated from the number of D4Z4. Using southern blot analysis, more than 90% of facioscapulohumeral muscular dystrophy patients have a smaller *Eco*RI fragment than 26 kb in our series, and the number of D4Z4 repeats is precisely counted by this polymerase chain reaction method. We conclude that this long polymerase chain reaction method can be used as an accurate genetic screening technique for facioscapulohumeral muscular dystrophy patients.

Keywords: Facioscapulohumeral muscular dystrophy; Chromosome 4q35; Genetic diagnosis; Southern blotting; PCR; *Eco*RI fragment; D4Z4

1. Introduction

Facioscapulohumeral muscular dystrophy (FSHD) is a common autosomal dominant muscular disorder characterized by its distinct clinical presentation. It often involves weakness and atrophy of facial muscles, followed by shoulder-girdle, the scapula fixators, and the upper arm muscles. Subsequently, pelvic girdle and lower limbs are also affected. About 20% of the patients eventually become wheelchair-bound by 40 years of age [1]. Difficulties of whistling, eye closure, or arm raising are common initial symptoms. Prominent scapular winging and horizontally positioned clavicles are also observed. Facial or shoulder girdle weakness usually appears during adolescence, but signs may be apparent on examination even in early childhood. Asymmetry of muscle involvement is often observed in apparently affected patients, but this is unrelated to handedness [2]. Weakness is relatively mild and the progression is usually slow with frequent association of subclinical hearing loss and retinal vasculopathy. The clinical diagnosis of FSHD is sometimes difficult because the onset of illness and the phenotypic expression is extremely variable, both within and between families [3,4].

The gene locus for FSHD has been identified on chromosome 4q35 wherein an array of tandem repeat units is located. Each repeat is a 3.3-kb *Kpn*I digestable fragment designated as D4Z4 (Fig. 1) [5–7]. The disease is usually associated with a deletion of this repeated region, however the responsible gene has not yet been identified, and the underlying molecular mechanism is still enigmatic. Southern blot analysis using the probe p13E-11 (D4F104S1) [6] is usually performed in the genetic diagnosis of FSHD. Normal individuals have *Eco*RI digested fragments containing D4Z4 repeats which varies from 40 kb to more than 300 kb in size, however, most of the FSHD patients have a smaller sized fragment from 10 to 35 kb. The clinical severity is often correlated to the fragment size, and patients with the smallest *Eco*RI fragment show very early onset and can be associated with epilepsy and mental retardation [8,9].

* Corresponding author. Tel.: +81 42 341 2712; fax: +81 42 346 1742.
E-mail address: hayasi_y@ncnp.go.jp (Y.K. Hayashi).

0960-8966/$ - see front matter © 2006 Elsevier B.V. All rights reserved.
doi:10.1016/j.nmd.2006.01.008

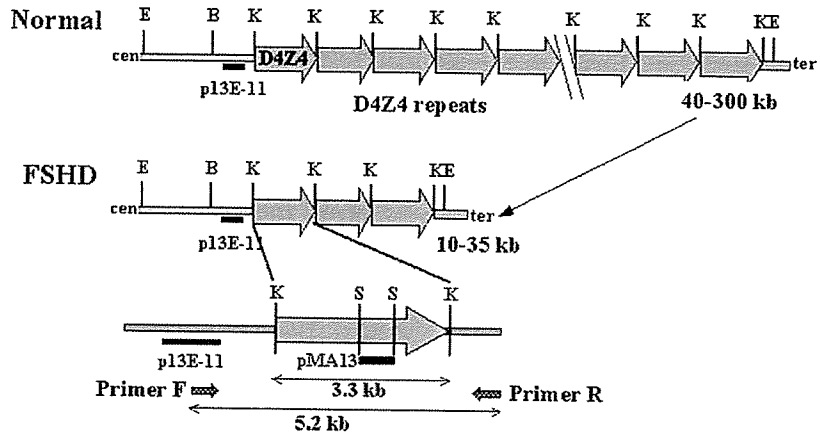

Fig. 1. A schematic diagram of the FSHD gene region on chromosome 4q35 showing the relative locations of primers and the probes used in this study. The primer set has been designed in the non-repeated region, and is expected to produce a 5.2 kb PCR amplified product when template genomic DNA contains one D4Z4 repeat. Cen, centromeric side of the gene; ter, telomeric side of gene; E, *Eco*RI; B, *Bln*I; K, *Kpn*I; S, *Sal*I.

Presently, the accuracy of the molecular diagnosis for FHSD using southern blot is up to 98% [10], however, several factors make this method cumbersome, and more than a week-length of time is required to obtain the results. In the conventional southern blotting method, it is difficult to resolve fragment size over 50 kb, and pulsed-field gel electrophoresis (PFGE) is sometimes taken together to increase resolution. Somatic and germline mosaicism is frequently observed in which more than three different sized *Eco*RI fragments on chromosome 4q are identified [11,12]. Furthermore, homologous 3.3-kb repeat-like sequences are also identified on many other chromosomes such as chromosomes Y and 3p [13,14]. In addition, chromosome 10q26 also contains 3.3-kb *Kpn*I digestable tandem repeats with 98% nucleotide identity to D4Z4 on chromosome 4 [15,16]. Consequently, there is a high incidence of inter-chromosomal exchange between 4q35 and 10q26, which is observed in about 20% of normal individuals [17,18]. In southern blot analysis, the probe p13E-11 used is not specific only to recognize *Eco*RI fragment from chromosome 4q but can also identify *Eco*RI fragment on chromosomes 10q26 and Y. This would require double restriction enzyme digestion using *Eco*RI and *Bln*I to be performed to distinguish 4q35-derived D4Z4 (*Bln*I-resistant) from 10q26-derived repeated units (*Bln*I-sensitive) [19]. From these complexities, there is an urgent need to develop a more simplified and reliable method for the diagnosis of FSHD.

Here, we introduce a new method to count the numbers of D4Z4 repeats on chromosome 4q35 by using long PCR amplification, which is quite useful for the rapid and accurate genetic diagnosis of FSHD.

2. Materials and methods

All clinical materials used in this study were acquired with informed consent. One hundred and five patients with a 4q-linked small *Eco*RI fragment from 10 to 35 kb (Table 3), and seven healthy individuals were examined. Genomic DNA was carefully and gently extracted from blood lymphocytes using a standard method. Southern blot analysis using the probe p13E-11 was performed as previously described [12].

For a long PCR amplification, a 50 μl reaction mixture was used. This mixture contains 400–600 ng of genomic DNA, 25 μl of 2× GC Buffer I (TAKARA BIO INC. Japan), 7.5 μl dATP/dTTP/dCTP mixture (10 mM each), 2.5 μl dGTP/7-deaza-dGTP mix (2:3), 1 μl (10 pM/μl) of each primers, and 0.5 μl (5 U/μl) LA Taq HS (TAKARA BIO). The primers were designed based on the human genomic sequences from GenBank (Accession Numbers D38025 and U74497). The primer sequences are F: 3′-GGCCAGAGTTT-GAATATACTGTGGTCATCTCTGCTCCAG-5′, R: 3′-CAGGGGATATTGTGACATATCTCTGCACTCATC. Amplification was performed using GeneAmp PCR System 9700 (PerkinElmer Japan Co., Ltd, Japan) with the following conditions; 1 min at 94 °C for the initial denaturation, followed by 10 cycles of 10 s at 98 °C and 20 min at 64 °C, and an additional 23 cycles of 10 s at 98 °C, 20 min with autoextension of 20 s per cycle at 64 °C, and 10 min at 72 °C for final elongation. The PCR products were separated by electrophoresis using 0.4% SeaKem HGT agarose gel (FMC BioProducts, ME) in 1× TAE with 0.5 μg/ml ethidium bromide at 3 h. High Molecular Weight DNA Marker (8.3–48.5 kb) (Invitrogen Japan K.K., Japan) and 1 kb plus ladder (Invitrogen) were used. The number of the 3.3 kb *Kpn*I repeated units in the FSHD gene region was calculated by the sequence data from GenBank (Accession Numbers D38024, D38025, and U74497).

In order to ascertain the specificity of the amplified products, we transferred the gels to Hybond N^+ (Amersham Biosciences, Japan) and overnight hybridization at 65 °C was performed with the ^{32}P-labeled probes of p13E-11 and pMA13 (1.3 kb *Stu*I fragment within a D4Z4 unit). The membrane was washed in a stringency of 2× SSC/0.1% SDS for 20 min at 65 °C for two times, followed by

Table 1
Comparison of long PCR and southern blot (SB) analyses

	PCR	SB
Template DNA (μg)	0.4	40
Enzyme digestion	No	*Eco*RI, *Bln*I
Gel size, concentration	11×14 cm, 0.4%	20×20 cm, 0.3%
Required time (h)		
PCR	11	0
Electrophoresis	3	68
Transfer	0	18
Hybridization	0	18
Detection	EB	RI
Total time required	<1 day	7–10 days
Accuracy (%)	90.1[a]	98 [10]

EB, ethidium bromide; RI, radio isotope.
[a] Estimated from the distribution of *Eco*RI fragment size in our series as described in Table 2.

autoradiography for 2 h using BAS2500 image analyzer (Fiji Photo Film, Japan).

3. Results

Table 1 shows the comparison of our newly developed long PCR method and the conventional southern blot analysis. This long PCR method is quite simple, requiring only a small amount of genomic DNA (1/100 of the quantity for southern blotting) and results are rapidly acquired overnight.

The long PCR method amplified five different sized products of 5.2, 8.5, 11.8, 15.1 and 18.4 kb which corresponded to the calculated size from the sequence data of the FSHD region containing one to five D4Z4 repeats, respectively (Fig. 2a, Table 3). These PCR products were not digested by *Bln*I, and were exclusively hybridized by the two probes of p13E-11 and pMA13 (data not shown). The same PCR method was performed on 10 individuals with a small *Eco*RI fragment (from 10 to 25 kb) on chromosome 10q26 but no amplified product was identified (data not shown).

Table 2 shows the distribution of the size of small *Eco*RI fragment on chromosome 4q of 263 FSHD families in our series. Table 3 shows the size of the PCR products, the calculated size of the *Eco*RI fragment, the range of the fragment size detected by southern blot analysis, and number of the patients. A 5.2 kb PCR product that contains one D4Z4 repeat was observed in eight patients with a *Eco*RI fragment from 10 to 11 kb. Sequence analysis confirmed that this 5.2 kb fragment contains one D4Z4 repeat on chromosome 4q35. An 8.5 kb band corresponding to the size with two D4Z4 repeated units was detected in 23 patients with 13–17 kb *Eco*RI fragment. An 11.8 kb product (three D4Z4 repeats) was seen in 26 patients with 16–19 kb fragment, a 15.1 kb fragment (four D4Z4 repeats) was seen in 24 patients with 18–22 kb fragment, and a 18.4 kb product (five D4Z4 repeats) was observed in six patients with 23–25 kb *Eco*RI fragment. The PCR products were amplified from all 87 DNA samples of the patients with an *Eco*RI fragment of 25 kb or less. However, DNA from normal individuals and FSHD patients with larger (≧26 kb) *Eco*RI fragments were not successfully amplified/detected by this long PCR method.

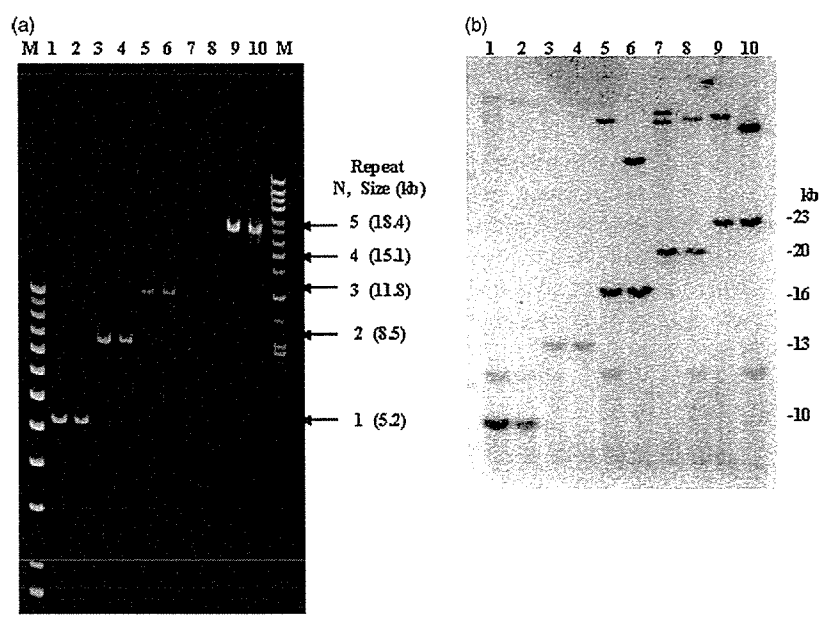

Fig. 2. Long PCR amplification and conventional southern blot analysis using genomic DNA from FHSD patients. (a) A 5.2 kb PCR product was detected on two patients with an *Eco*RI fragment of 10-kb (lane 1), or 11-kb (lane 2) as interpreted from our previous southern blot study. An 8.5-kb band was detected from two patients with a 13-kb (lane 3) or a 14-kb (lane 4) fragment, an 11.8-kb product from two patients with a 16-kb (lane 6) or a 17-kb (lane 7) fragment, a 15.1-kb product from a 20 or a 22 kb fragment, and an 18.4 kb fragment was identified from patients with a 24 and a 25 kb *Eco*RI fragment. These PCR products correspond to the size containing one to five D4Z4 repeated units. (b) Southern blot analysis using the same 10 samples in (a). The samples with the same size of the PCR products showed no difference of the *Eco*RI fragment size, although variable fragment size was previously interpreted.

Table 2
Distribution of *Eco*RI fragment size on chromosome 4q of 263 families in our series

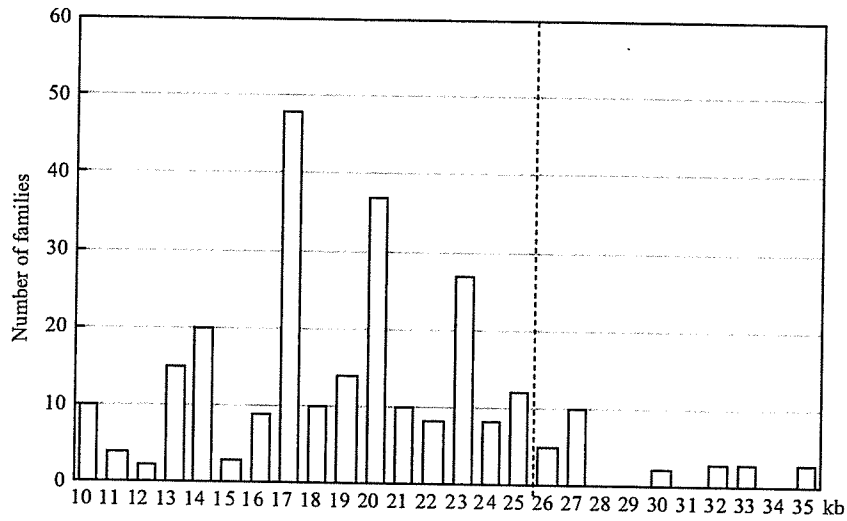

*Eco*RI fragments of <26 kb (dot line) can be amplified by long PCR analysis.

Estimated fragment size from the previous southern blot was not identical among the patients with same numbers of D4Z4 repeats. To determine the inter-individual variability of the fragment size, conventional southern blot analysis was repeated simultaneously. Notably, after the repeated southern blot technique, the *Eco*RI fragment size was similar when the D4Z4 number was the same and this result was consistent with the calculated size (Fig. 2b).

4. Discussions

In this study, we have successfully developed a new method for rapid and specific diagnosis of FSHD by counting the number of D4Z4 repeats via a long PCR amplification technique. This long PCR method can specifically amplify the repeated region from chromosome 4q up to 18.4 kb in size and countable from one to five D4Z4 repeated units.

Table 3
Comparison of the results of long PCR and southern blot (SB) analysis

Number of D4Z4 repeats	PCR product size (kb)	Calculated size of *Eco*RI fragment (kb)	Range of *Eco*RI fragment by SB (kb)	Number of patients examined by PCR
1	5.2	10.2	10-11	8
2	8.5	13.5	13–17	23
3	11.8	16.8	16–19	26
4	15.1	20.1	18–22	24
5	18.4	23.4	23–25	6
6	21.7	26.7	26–35	18 (No amplification)
7	25	30		
8	28.3	33.3		
9	31.6	36.6		

D4Z4 repeat has highly GC-rich sequence up to 73% [20]. Difficulties in PCR amplification often arise when GC content of the template DNA exceeds 50%. This difficulty in PCR amplification was overcame in our study by using thermo-stable long accurate Taq, 7-deaza-dGTP, and a higher denaturing temperature (98 °C) followed by a relatively higher annealing/extension temperature (64 °C) for 20 min with autoextension of 20 s per cycle. Therefore 73% of GC-containing repeated region of more than 18 kb in size was amplified with ease. The specificity of each PCR amplified product was ascertained by several ways. First, both probes (p13E-11 and pMA-13) that were used in the hybridization of the PCR products exclusively recognize fragments containing D4Z4 repeats. Second, the restriction enzyme *Bln*I did not digest the amplified fragments and confirmed that the product is apparently different from the repeats derived from chromosome 10q26, wherein 98% homologous *Kpn*I repeated units and franking sequences are known. Third, this long PCR method did not amplify *Kpn*I repeats from 10q26 even though the only difference is one different nucleotide from each of the primer region on 4q35. We also designed 10q-specific primer set and confirmed that only the 10q-derived repeats could be amplified by using this primer set.

The diagnosis of FSHD is sometimes difficult. Clinical symptoms and severity are quite variable between the patients even within the same family. Up to date, genetic diagnosis of FSHD is solely depended on the southern blot analysis since no responsible gene is yet identified within the candidate region. However, such procedure requires a large amount of DNA and would necessitate at least a week-time period to produce results. The requirement for such

amount of time for analysis dwells on the complexity of the experimental protocols in detecting the various fragments, the sizes ranging from 10 to 300 kb, as well as the determination of the existence of homologous regions on the other chromosomes. Determination of the size of *Eco*RI fragment is important since it is usually correlated to the clinical severity. However, identification of the precise fragment size is often difficult in the conventional southern blotting, since only very low concentrated gels of 0.3% is used to detect large sized fragment, and even minor changes in the experimental conditions would produce different results. In fact, in our very own series, DNA samples containing the same number of D4Z4 repeats showed the same *Eco*RI fragment size on one membrane although the estimated size in our previous analysis detected by different membranes were variable. Therefore, the number of D4Z4 units estimated from the *Eco*RI fragment size using Southern blotting could be misinterpreted from its actual number. From the result of the long PCR analysis, we concluded that the number of D4Z4 is countable from the size of PCR products, and the deletion of the FSHD region is certainly caused by the deleted integral number of D4Z4.

The number of D4Z4 is specifically countable up to five, which corresponds to the estimated *Eco*RI fragment of 10–25 kb in size. When no amplified product was obtained, southern blot analysis is required. In our series, 9.9% of the 4q-linked small *Eco*RI fragments have 26–35 kb as shown in Table 2, but the percentage may be greater in other countries. In the cases having deletion of p13E-11, no product can be obtained in this PCR analysis, since the forward primer is designed within this region. However, considering the complexity of the southern blot technique, this long PCR analysis is useful for the initial screening of the FSHD patients, and also the genetic test for the other family members with a known D4Z4 repeat numbers from 1 to 5 in an index patient. Obtaining accurate results rapidly is always beneficial for the patient, especially during prenatal test. From the economical point of view, PCR analysis is also beneficial since it costs 1/30–40 for the southern blot analysis.

Both primer sequences we used in this study are 4q-specific, and can amplify fragments even those with zero D4Z4 repeat, if any, producing an estimated 1.9-kb product. We also designed a primer set that can specifically amplify the repeated region on chromosome 10q. Theoretically, by using several combinations of these primers, we should be able to distinguish rare cases with short hybrid repeats on 4q or non-FSHD *Bln*I-resistant fragments on 10q. We concluded that the long PCR method could be used as an accurate genetic screening technique for FSHD.

Acknowledgements

We would like to thank Dr Mina Nolasco Astejada (NCNP) for critically reviewing the manuscript. This work was supported by Health and Labor Science Research Grants, Research on Psychiatric and Neurological Diseases and Mental Health, and The Research Grant (17A-10) for Nervous and Mental Disorders from the Ministry of Health, Labour and Welfare, Research on Health Sciences focusing on Drug Innovation from The Japan Health Sciences Foundation, Japan.

References

[1] Lunt PW, Harper PS. Genetic counselling in facioscapulohumeral muscular dystrophy. J Med Genet 1991;28:655–64.
[2] Tawil R, McDermott MP, Mendell JR, Kissel J, Griggs RC. Facioscapulohumeral muscular dystrophy (FSHD): design of natural history study and results of baseline testing, FSH-DY group. Neurology 1994;44:442–6.
[3] Lunt PW, Jardine PE, Koch M, et al. Phenotypic–genotypic correlation will assist genetic counseling in 4q35-facioscapulohumeral muscular dystrophy. Muscle Nerve 1995;2:S103–S9.
[4] Padberg GW, Frants RR, Brouwer OF, Wijmenga C, Bakker E, Sandkuijl LA. Facioscapulohumeral muscular dystrophy in the Dutch population. Muscle Nerve 1995;2:S81–S4.
[5] Upadhyaya M, Lunt P, Sarfarazi M, Broadhead W, Farnham J, Harper PS. The mapping of chromosome 4q markers in relation to facioscapulohumeral muscular dystrophy (FSHD). Am J Hum Genet 1992;51:404–10.
[6] Wijmenga C, Hewitt JE, Sandkuijl LA, et al. Chromosome 4q DNA rearrangements associated with facioscapulohumeral muscular dystrophy. Nat Genet 1992;2:26–30.
[7] Hewitt JE, Lyle R, Clark LN, et al. Analysis of the tandem repeat locus D4Z4 associated with facioscapulohumeral muscular dystrophy. Hum Mol Genet 1994;3:1287–95.
[8] Funakoshi M, Goto K, Arahata K. Epilepsy and mental retardation in a subset of early onset 4q35-facioscapulohumeral muscular dystrophy. Neurology 1998;50:1791–4.
[9] Miura K, Kumagai T, Matsumoto A, et al. Two cases of chromosome 4q35-linked early onset facioscapulohumeral muscular dystrophy with mental retardation and epilepsy. Neuropediatrics 1998;29: 239–41.
[10] Upadhyaya M, Cooper DN. Molecular diagnosis of facioscapulohumeral muscular dystrophy. Expert Rev Mol Diagn 2002;2: 160–71.
[11] Lemmers RJ, van der Wielen MJ, Bakker E, Padberg GW, Frants RR, van der Maarel SM. Somatic mosaicism in FSHD often goes undetected. Ann Neurol 2004;55:845–50.
[12] Goto K, Nishino I, Hayashi YK. Very low penetrance in 85 Japanese families with facioscapulohumeral muscular dystrophy 1A. J Med Genet 2004;41:e12.
[13] Clark LN, Koehler U, Ward DC, Wienberg J, Hewitt JE. Analysis of the organisation and localisation of the FSHD-associated tandem array in primates: implications for the origin and evolution of the 3.3 kb repeat family. Chromosoma 1996; 105:180–9.
[14] Ballarati L, Piccini I, Carbone L, et al. Human genome dispersal and evolution of 4q35 duplications and interspersed LSau repeats. Gene 2002;296:21–7.
[15] Deidda G, Cacurri S, Grisanti P, Vigneti E, Piazzo N, Felicetti L. Physical mapping evidence for a duplicated region on chromosome 10qter showing high homology with the facioscapulohumeral muscular dystrophy locus on chromosome 4qter. Eur J Hum Genet 1995;3:155–67.

[16] van Geel M, Dickson MC, Beck AF, et al. Genomic analysis of human chromosome 10q and 4q telomeres suggests a common origin. Genomics 2002;79:210–7.
[17] Matsumura T, Goto K, Yamanaka G, et al. Chromosome 4q;10q translocations; comparison with different ethnic populations and FSHD patients. BMC Neurol 2002;2:7.
[18] Lemmers RJ, van der Maarel SM, van Deutekom JC, et al. Inter- and intrachromosomal sub-telomeric rearrangements on 4q35: implications for facioscapulohumeral muscular dystrophy (FSHD) aetiology and diagnosis. Hum Mol Genet 1998;7: 1207–14.
[19] Deidda G, Cacurri S, Piazzo N, Felicetti L. Direct detection of 4q35 rearrangements implicated in facioscapulohumeral muscular dystrophy (FSHD). J Med Genet 1996;33:361–5.
[20] Lee JH, Goto K, Matsuda C, Arahata K. Characterization of a tandemly repeated 3.3-kb KpnI unit in the facioscapulohumeral muscular dystrophy (FSHD) gene region on chromosome 4q35. Muscle Nerve 1995;2:S6–S13.